HHS Public Access

Author manuscript

Nat Metab. Author manuscript; available in PMC 2022 May 29.

Published in final edited form as:

Nat Metab. 2021 December ; 3(12): 1608–1620. doi:10.1038/s42255-021-00487-4.

Serine catabolism generates liver NADPH and supports hepatic lipogenesis

Zhaoyue Zhang[1,2,*], **Tara TeSlaa**[2,*], **Xincheng Xu**[1,2], **Xianfeng Zeng**[1,2], **Lifeng Yang**[2], **Gang Xing**[3], **Gregory J Tesz**[3], **Michelle F Clasquin**[3], **Joshua D Rabinowitz**[1,2,†]

[1]Department of Chemistry, Princeton University, Princeton, New Jersey 08544, USA

[2]Lewis-Sigler Institute for Integrative Genomics, Princeton University, Princeton, New Jersey 08544, USA

[3]Pfizer Inc. Internal Medicine, Cambridge, MA 02139, USA

Summary

Carbohydrate can be converted into fat by *de novo* lipogenesis, a process upregulated in fatty liver disease. Chemically, *de novo* lipogenesis involves polymerization and reduction of acetyl-CoA, using NADPH as the electron donor. The feedstocks used to generate acetyl-CoA and NADPH in lipogenic tissues remain, however, unclear. Here we show using stable isotope tracing in mice that *de novo* lipogenesis in adipose is supported by glucose and its catabolism via the pentose phosphate pathway to make NADPH. The liver, in contrast, derives acetyl-CoA for lipogenesis from acetate and lactate, and NADPH from folate-mediated serine catabolism. Such NADPH generation involves the cytosolic serine pathway running in liver in the opposite direction observed in most tissues and tumors, with NADPH made by the SHMT1-MTHFD1-ALDH1L1 reaction sequence. SHMT inhibition decreases hepatic lipogenesis. Thus, liver folate metabolism is distinctively wired to support cytosolic NADPH production and lipogenesis. More generally, while the same enzymes are involved in fat synthesis in liver and adipose, different substrates are utilized, opening the door to tissue-specific pharmacological interventions.

†Correspondence and requests for materials should be addressed to J.D.R. (joshr@princeton.edu).

*Equal contribution

Author Contributions Statement

Z.Z., T.T. and J.D.R. came up with the general approach and experimental strategy. Z.Z and T.T. designed and performed the *in vivo* and *in vitro* experiments and data interpretation. X.X. performed folate species measurement. X.Z. performed acetate measurement. L.Y. contributed to the initial discovery of serine-mediated NADPH production in liver. G.X., G. J.T. and M.F.C. contributed to *in vitro* tracing experiments and GC-MS analysis. Z.Z., T.T., and J.D.R. wrote the manuscript with help from all authors.

Competing Interests Statement

G.X., G.J.T. and M.F.C. are current employees of Pfizer and may be Pfizer shareholders. J.D.R. is a consultant and received research funding from Pfizer and is an advisor and stock owner in Colorado Research Partners, L.E.A.F. Pharmaceuticals, Rafael Pharmaceuticals, Barer Institute and its subsidiaries, Serien Therapeutics, Toran, Kadmon Pharmaceuticals, and Agios Pharmaceuticals. J.D.R. is co-inventor of SHIN2 and related SHMT inhibitors, which have been patented by Princeton University. The remaining authors declare no competing interests.

Introduction

Lipids function as both structural molecules and energy storage in living cells. The main long-term energy store in mammals is triglycerides: fatty acids esterified to a glycerol backbone. To store ingested carbohydrates or protein as triglycerides, it is necessary to convert them into fatty acids. This occurs via the process of de novo lipogenesis[1].

Diverse disease processes are associated with increased de novo lipogenesis, including viral infection[2,3], cancer[4,5], and non-alcoholic fatty liver disease (NAFLD)[6,7]. Yet, the quantitative contribution of different nutrients to the acetyl-CoA and NADPH pools that support lipogenesis remains unclear.

De novo lipogenesis polymerizes acetyl-CoA molecules into fatty acid chains using the reducing power of NADPH. Acetyl-CoA can be produced from carbohydrate via pyruvate dehydrogenase in the mitochondria, from acetate in the cytosol, and from fatty acids and amino acids in mitochondria or peroxisomes. Lipogenesis, however, requires cytosolic acetyl-CoA. Mitochondrial acetyl-CoA can be transferred to the cytosol by first generating mitochondrial citrate which is then trafficked to the cytosol and converted into acetyl-CoA by ATP citrate lyase.

Isotope tracing into fatty acids provides a readout of the nutrient sources feeding into cytosolic acetyl-CoA. Such studies have illuminated complexities in carbohydrate conversion into fat. For example, fructose, a highly lipogenic carbohydrate, contributes to liver lipogenesis indirectly via microbiome-derived acetate[8,9,10]. Whether other nutrients, such as glucose, contribute to lipogenesis directly or indirectly via other circulating substrates such as lactate, and whether this varies across tissues, remains an open question.

The canonical cytosolic NADPH production route is the oxidative pentose phosphate pathway (oxPPP) and accounts for the bulk of NADPH production in cultured cancer cells and T cells[11–13]. Other cytosolic NADPH enzymes include malic enzyme (ME1), isocitrate dehydrogenase 1 (IDH1), and methylene tetrahydrofolate dehydrogenase 1 (MTHFD1) and 10-formyltetrahydrofolate dehydrogenase in folate metabolism[14,15]. Quantitative measurements of the sources of NADPH production for lipogenesis have not previously been made *in vivo.*

Here we utilize ^{2}H-stable isotope tracer technology to track NADPH production *in vivo* and employ it together with ^{13}C-tracing to determine the circulating sources of the tissue acetyl-CoA and NADPH used for lipogenesis. We find that circulating glucose provides both acetyl-CoA and NADPH for lipogenesis in brown adipose tissue. In contrast, the liver uses circulating acetate and lactate to make acetyl-CoA, and folate-mediated serine catabolism to generate NADPH. Genetic or pharmacological inhibition of folate-mediated serine catabolism suppresses hepatic lipogenesis.

Results

Lipogenesis is a substantial saturated fat source

Fatty acids can either be derived from diet or be synthesized from other nutrients by *de novo* lipogenesis. Those that can be synthesized by *de novo lipogenesis* are called non-essential. Two non-essential fatty acids are highly abundant in mammals: palmitate (C16:0; 16 carbons and zero double bonds) and oleate (C18:1). Together with the essential fatty acid linoleate (C18:2)[16], these three fatty acids together account for roughly 80% body fat[17] (Extended Data Fig. 1a, b). We sought to determine whether lipogenesis accounts for a meaningful fraction of tissue fatty acids and in which tissues lipogenic flux occurs.

To quantify the fraction of tissue fat from lipogenesis in mice fed standard carbohydrate-rich lab chow, we used isotope-labeled water (20% D_2O)[18–23]. Labeled water drinking did not perturb body weight (Extended Data Fig. 1c). Deuterium from heavy water is stably incorporated into newly synthesized fatty acids both directly and via NADPH[24]. Serum labeling of saponified fatty acids, which reflects both free fatty acids and those covalently embedded in phospholipids and triglycerides, reached steady state with a half-time of around 1 week; white adipose tissue reaches steady state more slowly (Extended Data Fig. 1d). At steady state, the fraction of each fatty acid coming from synthesis, as opposed to diet, was determined by fitting the observed mass isotopic distribution (Fig. 1a). Labeling of saponified palmitate was extensive across serum and all tissues, while, as expected, linoleate was completely unlabeled (Fig. 1b). Quantitative analysis, summing *de novo* fatty acid amounts across tissues, revealed that most fatty acids in mouse (~80%) come from diet[25], but in standard carbohydrate-rich (62.1% calorie) chow-fed mice about half of saturated fat is synthesized *de novo* (Fig. 1c).

A challenge in interpreting long term D_2O labeling experiments is that fat can be exchanged between organs, and indeed, the steady-state measurements revealed nearly indistinguishable palmitate labeling across tissues (Fig. 1b, Extended Data Fig. 1e). To elucidate the organs responsible for lipogenesis, we performed 6 – 12 h intravenous infusions of D_2O[26] which provide sufficient enrichment to detect labeling in both NADPH and palmitate with minimal stress to animal, and during which D_2O enrichment increased linearly (Extended Data Fig. 1g). Measurements taken throughout the day at 6 h intervals confirmed that lipogenesis in mice occurs more rapidly in the night, when mice are more active and eat more (Extended data Fig. 1h). Overnight infusions showed greatest saponified fatty acid labeling in liver and brown adipose tissue (Fig. 1d, Extended Data Fig. 1i,j), consistent with liver's canonical lipogenic role and brown adipose lipogenesis induction in mice housed at room temperature[27]. Only in these two tissues did labeling exceed that of circulating fat (Fig. 1d, Extended Data Fig. 1i,j). This does not rule out the possibility of *de novo* synthesis in other tissues such as white adipose, where slow fractional labeling can occur due to the large pre-existing fat pool (indeed, refeeding after fasting for 24 h increased fat labeling from D_2O in white adipose tissue but not liver or brown adipose[28], Extended Data Fig. 1k). Nevertheless, these data show unambiguously that liver and brown adipose tissue can actively engage in *de novo* lipogenesis.

Liver and adipose use different substrates to make fat

Next, we focused on identifying the carbon sources supporting palmitate synthesis in liver and brown adipose. To this end, we infused various ^{13}C-labeled nutrients and monitored circulating nutrient and saponified tissue palmitate labeling. Tracers were infused at rates that did not substantially elevate the infused metabolite's levels (Extended Data Fig. 2a,b,c, Methods Table 1). In the circulation, labeling was observed both in the infused tracer and downstream metabolites. To account for dilution of tracer by absorbed food, serum samples were collected both from the tail vein and from the portal vein that carries blood from the intestine to the liver (Extended Data Fig. 2d,e). Palmitate was labeled from both glucose and lactate in both the liver and brown adipose, whereas labeling from acetate was prominent only in the liver (Fig. 2a,b; Extended Data Fig. 2f).

The relative labeling from glucose and lactate differed between liver and brown adipose, with lactate labeling more fatty acid in liver and glucose labeling more in adipose (Fig. 2a,b). Because glucose and lactate interconvert via glycolysis and gluconeogenesis, infusion of either substrate labels both in the circulation[26] (Fig. 2c; Extended Data Fig. 2d,e). Accordingly, even if only one of the substrates is used by a tissue to drive lipogenesis, we will observe labeling from infusion of either substrate. By monitoring the extent of tissue palmitate labeling from infusion of each substrate, as well as the extent of cross-labeling between the substrates, the direct contribution of each substrate can be determined. Specifically, in each tracer experiment, the observed fat labeling reflects the sum of each substrate's direct fat contribution multiplied by its circulating labeling. The resulting equations can be solved for each substrate's direct contribution by a linear algebra calculation[26,29]. This analysis revealed that, while glucose and lactate both directly contribute to brown adipose lipogenesis, glucose contributes indirectly to hepatic lipogenesis through circulating lactate (Fig. 2d,e)[26,30]. Importantly, there is no discernible direct circulating glucose contribution to liver fat synthesis (Fig. 2d). Consistent with this, lactate but not glucose contributed to TCA cycle intermediates in liver tissue slices (Extended Data Fig. 3). Collectively, these findings support lactate (the classical liver gluconeogenic substrate[31,32]) and acetate (the substrate of the pro-lipogenic and cancer-supporting enzyme ACSS2[33–37]) as being primary lipogenic inputs to liver.

NADPH in brown adipose comes from the oxPPP

Much of the energy in fatty acids comes from NADPH[1], which donates hydrogen to drive acetyl reduction. The canonical cytosolic NADPH production route is the oxidative pentose phosphate pathway (oxPPP)[1,38,39]. To investigate whether NADPH produced by the oxPPP supports hepatic lipogenesis, we began by studying cultured primary hepatocytes. Hepatocytes (both in liver and primary cells in culture) only weakly express oxPPP enzymes[40]. OxPPP flux can be measured *in vitro* by monitoring the differential $^{14}CO_2$ release from [1- ^{14}C]glucose (oxPPP tracer) and [6-^{14}C]glucose. The two tracers produce $^{14}CO_2$ identically when glucose is catabolized in the TCA cycle, with greater $^{14}CO_2$ release from [1- ^{14}C]glucose quantitatively reflecting oxPPP flux (Fig. 3a). While hepatocellular carcinoma cells (HepG2) manifested strong oxPPP flux as expected for cancer cells, the absolute oxPPP flux in primary mouse hepatocytes was undetectable (Fig. 3b–c).

Flux from the oxPPP can also be traced into NADPH's redox active hydrogen using glucose deuterated at C1 or C3 (Fig. 3d). Such labeling can be read out in NADPH itself or in downstream products, such as newly synthesized fatty acids. In prior work in cultured cancer cells, we found that NADPH deuterium labeling from the oxPPP is incomplete due to Flavin enzyme-mediated exchange of NADPH's active hydrogen with water[14,24]. Correcting for such exchange, which can be monitored using D_2O, revealed that the oxPPP is the main cytosolic NADPH source in most cultured cancer cells[11,39,41]. Whether non-transformed lipogenic cells mainly use the oxPPP to generate NAPDH remains unclear. Using [3-^{2}H]glucose we found that, unlike HepG2 cells, primary hepatocytes manifest almost no NADPH and fat labeling from oxPPP, suggesting the predominance of alternative NADPH production pathways[15] (Extended Data Fig. 4a–e).

We next translated the ^{2}H-tracing technology *in vivo* by infusing mice with [1-^{2}H]glucose overnight. We observed strong labeling of brown adipose palmitate (Fig. 3e), confirming the effectiveness of this tracing strategy. After correcting for the fraction of NADPH's active hydrogen that is exchanged with water and the extent of tissue glucose labeling (Fig. 3e, Extended Data Fig. 4f), we found that the oxPPP accounts for nearly all cytosolic brown fat NADPH production (Fig. 4f right). Liver fat was not labeled, however, indicating that liver relies on alternative NADPH sources (Fig. 3e,f). These results agree with negligible expression of *G6pd* in hepatocytes, and greater expression in brown adipose, white adipose, and leukocytes including liver resident T-cells and Kupffer cells[42–46]. Thus, the oxPPP is the main source of brown adipose NADPH.

Hepatocytes prefer glutamine for TCA only in vitro

Multiple studies have identified isocitrate dehydrogenase 1 (IDH1) and malic enzyme 1 (ME1) as important cytosolic NADPH producers in lipogenic cells[15,47,48]. Consistent with this, lysates of primary hepatocytes showed substantial ME1 and especially IDH1 activity (Extended Data Fig. 4d). In addition, [2,3,3,4,4-^{2}H]glutamine labeled the redox-active hydrogen of NADPH and downstream fat in primary hepatocytes, reflecting cytosolic NADPH production from ME1 and/or IDH1 (Extended Data Fig. 4a,b). After correcting for hydrogen-deuterium exchange based on experiments with D_2O, the combined contribution of the oxPPP, malic enzyme, and IDH in primary hepatocytes was, however, less than 50% (Extended Data Fig. 4e).

To determine if IDH1 and ME1 are major sources of liver NADPH *in vivo*, we attempted [2,3,3,4,4-^{2}H]glutamine infusion. Unfortunately, there was extensive deuterium loss between glutamine and malate/isocitrate, rendering the resulting lack of labeling in palmitate uninformative (Extended Data Fig. 4h–k). To determine why [2,3,3,4,4-^{2}H]glutamine tracing was successful in cultured hepatocytes but not *in vivo*, we performed [U-^{13}C]glutamine tracing to analyze the TCA cycle. We found that glutamine is the predominant hepatocyte TCA substrate *in vitro* but not *in vivo*[49] (Extended Data Fig. 4a,k). Alternative approaches to label the relevant hydrogen atoms of malate and isocitrate were unsuccessful even in cultured hepatocytes (Extended Data Fig. 4l).

Serine catabolism feeds liver NADPH production

The above findings suggest that the oxPPP, malic enzyme, and IDH collectively account for no more than half of cytosolic NADPH production in primary hepatocytes. Serine catabolism is a potential alternative NADPH source, which drives mitochondrial NADPH production for redox defense during cancer metastasis[50]. To date, however, serine catabolism has not been shown to be a physiologically relevant contributor to cytosolic NADPH. We explored whether serine might contribute to NADPH production in primary hepatocytes using [2,3,3-^{2}H]serine (Fig. 4a). In cultured hepatocytes, we observed NADPH and downstream fat labeling from [2,3,3-^{2}H]serine (Extended Data Fig. 4a,b,e).

We next turned our attention to whether serine contributes to NADPH production in the liver *in vivo*. Infusion of [2,3,3-^{2}H]serine at 20 nmol/min/gram bodyweight did not detectably label palmitate in brown fat (Fig. 4b); nor did it label liver acetyl-CoA or related liver metabolites (Extended Data Fig. 5b). Impressively, however, we obtained substantial labeling in NADPH's active hydrogen and palmitate in the liver (Fig. 4b,c).

As serine catabolism had not been previously established as a physiological NADPH source, to assess the robustness of serine's hepatic NADPH contribution we replicated the ^{2}H-serine infusion across an 8-fold range of rates. The lowest infusion rates were minimally perturbative, and the highest rates increased serum serine concentration by 2-fold but gave enough labeling to more readily analyze downstream metabolites (Extended Data Fig. 5a). In brown fat, palmitate labeling from ^{2}H-serine was minimal even at the highest infusion rate. In contrast, in liver, labeling was detected across all infusion rates in direct proportionality to the administration rate of labeled serine (Fig. 4d). The observed labeling in liver reflects a consistent normalized contribution from [2,3,3-^{2}H]serine to hepatic fat (Fig. 4e). The highest serine infusion rate (40nmol/min/gram bodyweight) gave substantial labeling in both fat and NADPH's redox active hydrogen, with the extent of NADPH and fat labeling in quantitative agreement (Fig. 4f). The carbon and hydride contributions of different substrates to fat, including serine's NADPH contribution, were consistent across male and female mice (Extended Data Fig. 6). Thus, serine provides hydride to NADPH that contributes to liver lipogenesis (Fig. 4f–g)

The SHMT1-MTHFD1-ALDH1L1 folate pathway makes liver NADPH

We next sought to determine the pathway linking serine to NADPH and liver fat synthesis, hypothesizing folate-mediated cytosolic serine catabolism via the SHMT1-MTHFD1-ALDH1L1 reaction sequence[14]. Both MTHFD1 and ALDH1L1 are capable of making NADPH, although neither had been shown to do so in a physiological context previously[51]. Indeed, in most cells, MTHFD1 runs in the NADPH-consuming direction[52]. To assess the direction of one-carbon flux *in vivo,* following [2,3,3-^{2}H]serine infusion, we monitored the labeling of 5-methyl-THF. Serine catabolism in mitochondria, followed by re-assimilation of the resulting formate in the cytosol, results in M+1 5-methyl-THF and consumes cytosolic NADPH. In contrast, cytosolic serine catabolism generates M+2 5-methyl-THF and can support cytosolic NADPH production[53] (Fig. 5a). We observed a predominance of M+1 5-methyl-THF in most tissues, but a strong M+2 5-methyl-THF signal specifically in liver, indicative of SHMT1-mediated cytosolic serine catabolism (Fig. 5b, Extended Data Fig. 7a).

To confirm that the observed NADPH and fatty acid labeling in liver is derived from cytosolic serine catabolism, we carried out [2,3,3-^{2}H]serine tracing in *Shmt1* whole-body knock-out mice, which are viable, fertile, exhibit no major metabolic defects[51,54] but are slightly insensitive to insulin (Extended Data Fig. 7b). These mice showed a complete loss of M+2 5-methyl-THF (Fig. 5c), confirming functional ablation of SHMT1 enzymatic activity. We also observed an 80% drop in NADPH and palmitate labeling from serine in the liver (Fig. 5d,e; Extended Data Fig. 7c,d,g). Thus, SHMT1-driven serine catabolism is a substantial NADPH source for hepatic lipogenesis.

In the absence of SHMT1, folate metabolism can contribute to hepatic NADPH production via ALDH1L1, which can oxidize formyl-THF[55]. Serine can contribute to cytosolic formyl-THF either via SHMT1-MTHFD1 or via the mitochondrial enzymes SHMT2-MTHFD2-MTHFD1L[56–58]. To probe the significance of ALDH1L1, we carried out tracer studies with [^{2}H]formate, observing substantial NADPH and fat labeling, although less than that from deuterated serine (Extended Data Fig. 7e,f). Thus, both the SHMT1-MTHFD1 reaction sequence, and downstream ALDH1L1 which can also be fed via the SHMT2 pathway, contribute to serine-driven hepatic NADPH production.

To more completely inhibit serine's hepatic NADPH contribution, we used a pharmacological dual SHMT1/2 inhibitor, SHIN2[53]. Treatment with SHIN2 markedly decreased both NADPH and palmitate labeling from [2,3,3-^{2}H]serine in liver (Fig. 5d,e). Labeling from [^{2}H]formate, which feeds directly into the formyl-THF pool[55] and can generate cytosolic NADPH via ALDH1L1, was maintained (Extended Data Fig. 7f).

Inhibition of serine catabolism decreases liver lipogenesis

Finally, we assessed whether manipulation of serine-driven NADPH production could impact the overall rate of hepatic lipogenesis. D_2O tracing revealed that both *Shtm1* knockout and pharmacological SHMT1/2 inhibition significantly decreased hepatic but not brown adipose fat synthesis (Fig. 5f, Extended Data Fig. 8a–g). Decreased lipogenesis in response to SHMT1/2 inhibition was observed regardless of method of D_2O delivery (intravenously or by IP injection) (Extended Data Fig. 8c, d). Consistent with liver making circulating fat, *Shmt1* knockout decreased serum fat labeling from both [2,3,3-^{2}H]serine and D_2O. Labeling in some other tissues (e.g. lung, bone marrow) also decreased, likely because they acquire fat made originally in the liver from the circulation (Extended Data Fig. 7g; Extended Data Fig. 8h). Perhaps due to compartmentation and/or measurement imprecision, we did not detect a statistically significant impact of S*hmt1* knockout or SHMT1/2 inhibition on overall tissue NADPH, serine, or glutathione, but we did observe increased oxidized:reduced glutathione ratio in response to SHMT1/2 inhibition (Extended Data Fig. 8i–n). During re-feeding after fasting, liver lipogenic flux was also decreased in the *Shmt1* knockout mice (Extended Data Fig. 8o). These data combined indicate that inhibition of serine catabolism can decrease hepatic lipogenesis.

To determine if there is compensation from other NADPH sources, we used the oxPPP tracer [1-^{2}H]glucose in the *Shmt1* knockout mice but did not observe liver labeling fat (Extended Data Fig. 9a). Thus, SHMT1 loss does not induce liver oxPPP activity. Furthermore, we did

not observe changes in expression of other lipogenic and NADPH-producing enzymes like malic enzyme (Extended Data Fig. 9b,c).

Rates of *de novo* lipogenesis increase in fatty liver disease and in response to diets high in sweets (fructose or sucrose)[6,8,59–61]. Therefore, we analyzed the role of liver SHMT1-MTHFD1-ALDH1L1 in lipogenesis induced by sucrose water drinking, mimicking human soda consumption (Fig.6a scheme). After 4 weeks of 20% sucrose water, as expected, lipogenesis flux increased significantly in liver but not in brown adipose tissue (Fig. 6a; Extended Data Fig. 10a, b). The enhanced hepatic lipogenesis resulted in increased serum fat labeling, which exceeded brown adipose fat labeling, making it infeasible to quantify local brown fat lipogenesis rate or inputs in this condition, as the observed labeling could be coming from uptake of circulating fat (Extended Data Fig. 10b). Lipogenesis in the liver, however, still utilized NADPH produced by serine catabolism (Fig. 6b).

Finally, we examined whether sucrose-induced liver lipogenesis could be mitigated by inhibition of serine catabolism. After extended sucrose water drinking, we administered the SHMT1/2 inhibitor SHIN2 IV for 36 h (Fig. 6c scheme). D_2O infusion during the last 12 h of the inhibitor treatment revealed a significant decrease in hepatic lipogenesis[62] (Extended Data Fig. 10c, Fig. 6c). Consistent with this, in both liver and serum, we also observed decreased levels of triglyceride species containing saturated fatty acids (Fig. 6d). Moreover, circulating saponified fatty acids, indicative of total circulating fat, decreased (Extended Data Fig. 10d).

Discussion

The past century of biochemical research has revealed the enzymatic network of metabolism in exquisite detail. Yet the way that these enzymes work together within and across different tissues remains less fully defined. For *de novo* lipogenesis, despite its medical importance, the upstream precursors had not been quantitatively assessed. Using stable isotope tracing we found that circulating glucose supplies both carbon and hydride for lipogenesis in brown adipose tissue. In the liver, however, other substrates were used for both roles, with serine catabolism emerging as an unexpected cytosolic NADPH source.

Serine catabolism through one-carbon metabolism is important for organismal development, cancer cell growth, and immune function[63–66]. The enzymes important for these functions are, however, mitochondrial (e.g. SHMT2, MTHFD2, or MTHFD1L)[50,52,54,67,68], with the physiological function of cytosolic SHMT1 a long-standing puzzle[54]. The present data show that, while most tissues generate 1C units from serine via the mitochondrial pathway, the liver uniquely relies on cytosolic serine catabolism. Flux running from serine through SHMT1-MTHFD1-ALDH1L1 net generates two NADPH per serine which support hepatic lipogenesis. Our flux measurements align with enzyme expression data with SHMT1, MTHFD1 and ALDH1L1 all highly expressed in liver. Moreover, expression of the mitochondrial serine catabolic enzymes MTHFD2 and MTHFD1L is low in the liver[40]. This precludes flux in liver from mitochondrial serine catabolism to cytosolic 10-formyl-THF, and thereby favors coupled cytosolic formyl-THF and NADPH production via SHMT1-MTHFD1. Together with low liver G6PD expression and oxPPP flux, these data

suggest a primary role of gene expression in controlling *in vivo* NADPH production routes. This unique directionality of hepatic one-carbon metabolism may be related to the liver's redox requirements for drug detoxification, cholesterol production and de novo lipogenesis.

To measure de novo lipogenesis, a standard methodology is tracking passage of deuterium from deuterated water into fat. Typically, this is done by oral or IP administration of deuterated water[69–71]. Here, however, we also used intravenous infusion. For animals with intravenous access, this allows delivery of a large volume of D_2O in a temporally controlled manner without the animal handling (and potential associated stress-induced alterations in lipogenesis) associated with IP dosing[70,72–74]. The resulting increased deuterium labeling enabled label detection directly in NADPH, in addition to in fat[24].

De novo lipogenesis is a target of interest for treating cancer[75] and non-alcoholic fatty liver disease[76]. To date, drug development efforts have focused on the core fatty acid biosynthetic enzymes, acetyl-CoA carboxylase (ACC1) and fatty acid synthase (FASN)[76], which are required for fat synthesis across all tissue types and tumors. ACC1 inhibitors have proven effective in decreasing lipogenesis but cause hypertriglyceridemia in both rodents and humans[77,78]. While the mechanism underlying the hypertriglyceridemia remains unclear, a concern with general lipogenesis inhibition is that excess carbon must ultimately be safety stored.

The physiological location for long-term carbon storage is adipose[79,80]. Accordingly, it is conceptually appealing to selectively block lipogenesis in the liver or in tumors, while retaining adipose lipogenesis. The present data show that, despite *Acss2* being widely expressed[40], acetate is a liver-specific lipogenic carbon source. Moreover, serine catabolism is a liver-specific cytosolic NADPH source. The associated dependency of hepatic but not adipose lipogenesis on ACSS2 and SHMT1 offers a potential strategy to inhibit preferentially hepatic lipogenesis. Further work is merited to assess risks and benefits of this approach in relevant disease states.

Methods

Mouse experiments

Mouse work was approved by the Princeton University Institute Animal Care and Use Committee (protocol no. 2032). Mice were housed under normal light cycle (lights on 8:00–20:00) and fed standard chow diet, PicoLab Rodent 20 (Lab Diet, cat. no. 5053), *ad libitum* unless otherwise noted. The standard chow contains 5% fat by weight (1% saturated fat), while a typical western diet contains 21% fat by weight (13% saturated fat). Eight-week-old wild type C57BL/6NCrl mice were purchased from Charles River Laboratories (strain code #027). Mice were allowed at least 5 days[81] of acclimation to the facilities prior to experimentation and were randomly chosen for different experimental conditions. No blinding was implemented. Drinking water, 20% deuterium water (Cambridge Isotopes, cat. no. DLM-6) and 20% sucrose water (Sigma Aldrich, cat. no. 84097) experiments started one week after arrival and lasted for 4 weeks or more, with tail vein blood for circulating fatty acid labeling collected weekly. For experiments involving 24 h fasting, food was removed at 20:00 and replaced at 20:00 +1 day, followed by refeeding with tracing.

Intravenous tracer infusions were done on mice after in-house right jugular vein catheterization. During infusions, mice are single housed and can move freely in the cage with normal access to food and water. Mice were 10–16 weeks old at the time of isotope infusion measurements. Unless otherwise indicated, infusions were performed during the dark cycle from 20:00 to 8:00 +1 day, during which time the mice are more active, feed more, and synthesize more fat. All tracers were dissolved in 0.9% saline. Tracer concentrations and infusion rates are shown in Table 1.

Tail blood was collected prior to sacrifice to measure circulating labeling via tail snip. Blood samples were kept on ice to coagulate and then centrifuged at 4°C to separate serum. Thereafter, mice were anesthetized with isoflurane, opened, and resected. The portal vein was cut, and portal blood was taken with pipet. Then 12 tissues were collected in the following order: liver, spleen, pancreas, kidney, small intestine, perigonadal white adipose tissue, inguinal white adipose tissue, quadriceps, lung, heart, brown adipose tissue, and brain. All tissues were immediately clamped with a liquid nitrogen temperature Wollenberger clamp and dropped in liquid nitrogen. After tissue collection, mice were sacrificed by cervical dislocation.

For intraperitoneal D_2O injections for measurement of de novo lipogenic flux, 33 μl per gram body weight of D_2O saline (0.9% NaCl) was injected at 20:00, and mice were provided drinking water with 5% deuterium water to maintain enrichment throughout the experiment. At 8:00 +1 day, serum was collected via tail snip, mice were anesthetized with isoflurane and tissues were collected as described above. Mice were single housed for a week prior to the experiment and between 10–16 weeks of age at the time that the experiment was performed.

Shmt1 knockout mice and pharmacological SHMT inhibition

The whole-body *Shmt1* knockout mice were a generous gift from Prof. Patrick J. Stover[54] and bred at Princeton for more than 10 generations as heterozygotes on the C57Bl/6 background. Homozygotes knockout progeny and littermate wild type control mice were used in experiments. For SHMT1 &2 inhibition experiments, the small molecule SHMT inhibitor SHIN2 was dissolved in 20% 2-hydroxypropyl-β-cyclodextrin as a 20mg/mL stock and diluted in 0.9% saline to the desired concentration. Drug or vehicle control was intravenously infused, sometimes together with tracers, through the jugular vein catheter at an infusion rate of 3.33mg/kg/h, which is equivalent to 40mg/kg SHIN2 over a 12-hour period.

Primary hepatocyte collection and cell culture

Primary hepatocytes were isolated from wild type C57BL/6 mice[82] and cultured in high glucose (4.5g/L) DMEM medium supplied with 1% Pen Strep, 100 nM insulin, 100 nM dexamethasone, and 1% glutamax. Primary hepatocytes were cultured in collagen-coated 6-well plates in 37°C, 5% CO_2 incubator. HepG2 cells were obtained from ATCC (ATCC HB-8065) and cultured in DMEM with 10% FBS. For labeling experiments, primary hepatocytes were isolated, cultured overnight, and used the next morning. For isotope labeling experiments, HepG2 cells were changed into the same condition as primary

hepatocytes 24 h prior to start of tracing. Medium was aspirated and replaced with otherwise identical pre-warmed medium containing the indicated isotope tracer in place of the corresponding unlabeled nutrient. Duration of labeling was 2.5 h for soluble metabolite measurement and 6 h for fat measurement. To harvest metabolites, media was aspirated and 500 μL −20 °C 40:40:20 methanol: acetonitrile: water with 0.5% formic acid was directly added, then neutralized immediately with 15% NH_4HCO_3 solution (2.2% v/v of extraction buffer). Cells were collected with a scraper and transferred together with extraction buffer into a 1.5 mL vial on dry ice. Samples were incubated on dry ice for 1–1.5 h then thawed on ice and centrifuged at 4 °C, 16,000 x g for 10 min. Supernatant was then directly analyzed by LC-MS.

Liver slice experiments

Wild type C57BL/6 mice were anesthetized with isoflurane. Livers were resected and liver tissue slices from different lobes were collected with combined two blades and immediately transferred into 6-well plates with Krebs-Ringer buffer (with 10 mM glucose, 3 mM sodium lactate, 0.8 mM sodium acetate and 1 μM insulin) with the metabolites replaced by labeled forms as indicated. Then the slices were cultured in an incubator at 37°C, 5% CO_2 for 2h or 6h. Thereafter, tissue slices were washed with ice-cold PBS, frozen on dry ice, ground, and metabolites extracted.

Enzymatic activity assays

A diaphorase-resazurin-coupled biochemical assay was used to detect G6PD, IDH1, ME1 enzyme activity in cell lysates. Cytosolic proteins were isolated by subcellular protein fractionation kit (Thermo, 78840). 2% v/v of cytosolic lysate was mixed with buffer (50 mM Tris pH = 7.4, 5 mM $MgCl_2$, 1 mM resazurin, 0.25 mM $NADP^+$, 0.1 U mL^{-1} diaphorase and 0.1 mg mL^{-1} bovine serum albumin). To this mixture, substrate (glucose-6-phosphate for G6PD, isocitrate for IDH1 and malate for ME1) was added to a final concentration of 1 mM to initiate reactions. The kinetics of NADPH production were recorded by relative fluorescent unit measurement using a plate reader. The excitation wavelength was 540 nm and emission wavelength 590 nm.

Radioactive CO_2 release from oxPPP pathway

$^{14}CO_2$ release from [1- ^{14}C]glucose and [6-^{14}C]glucose was used to measure oxPPP flux as previously described[11,14]. Briefly, cells were grown in rubber stopper-sealed tissue culture flasks with DMEM containing 0.5 μCi mL^{-1} [1-^{14}C]glucose or [6-^{14}C]glucose. 150 μL of 10 M KOH was added to a center well (Kimble Chase) containing a piece of filter paper. After 16 h, cell metabolism was quenched, and CO_2 was released by injecting 1 mL 3 M acetic acid through the stopper. Everything in the center well was transferred into a scintillation vial for counting. Absolute flux was calculated as previously described[11,14].

qRT-PCR protocol

Liver tissue was weighed out and RNA isolated with TRIzol reagent (Life Technologies). 1 mL of TRIzol reagent was used per 50 mg of tissue and RNA was extracted according to manufacturer instructions. RNA was converted to cDNA with iScript (Bio-Rad). qRT-PCR

was performed with ViiA 7 system using Fast SYBR green (Applied Biosystems). Primers were generated as custom DNA oligos from Integrated DNA Technologies (IDT) and sequences were either from Roche Universal library or taken from the literature as indicated in Supplementary Table 1[77]. All data was normalized to the expression of ribosomal protein lateral stalk subunit P0 (*Rplp0*) as a control.

LC-MS sample preparation

Tissue samples were stored at ≤ −70°C. Tissues were pulverized using a Cryomill (Retsch). 10–20 mg of the resulting powder was weighed into a pre-cooled tube for extraction.

Soluble metabolites extraction was done by adding −20 °C 40:40:20 methanol: acetonitrile: water with 0.5% formic acid to the resulting powder (40 μL solvent/mg tissue) and the samples were first vortexed for 5 s and then neutralized immediately with 15% NH_4HCO_3 solution (2.2% v/v of extraction buffer). All samples were then vortexed again for 10 s, incubated at −80°C for 1 – 1.5 h, thawed on ice and then centrifuged at 4°C, 16,000 x g for 10 min. Supernatant was transferred to LC-MS vials for analysis. The acid and associated neutralization are important for NAD(P)(H) measurement and were omitted for ^{13}C-labeled samples where NAD(P)(H) measurement was not the focus.

Saponified fatty acid extraction of tissue was done by adding 1 mL of 0.3 M KOH in 90:10 MeOH/H_2O to the weighed tissue powder. After transferring the resulting mixture to a 4 mL glass vial, saponification was done at 80 °C in water bath for 1 h. Then samples were cooled to room temperature, neutralized with 100 μL pure formic acid and extracted with 1 mL of hexane. The hexane layer was transferred to another glass vial, dried down under N_2, and resuspended in 1:1 methanol: acetonitrile (100 μL/mg tissue; 40 μL/μL serum) for LC-MS analysis.

Serum samples were collected by centrifuging blood at 16,000 x g at 4 °C for 10 min. Then serum was extracted as above for both water-soluble metabolites (final volume: 30 μL methanol per 1 μL serum) and saponified fatty acids (final volume: 40 μL 1:1 methanol:acetonitrile per 1 μL serum).

Acetate labeling in serum was measured with a derivatization method: 5 μL serum was added into 100 μL of a mixture of 12 mM 1-ethyl-3-(3-dimethylaminoproryl)carbodiimide (EDC), 15 mM 3-nitrophenylhydrazine, and pyridine (2% v/v) in methanol, incubated at 4 °C for 1 h, and centrifuged for 10 min at 16,000 x g. Then the supernatant was quenched with 0.5 mM 2-mercaptoethanol and 0.1% formic acid in water and directly analyzed by LC-MS analysis[83].

Folate species were also measured by a derivatization method[84]. 20 mg of tissue was extracted with 1 mL of 1:1 MeOH:H_2O with sodium ascorbate (25 mM) and NH_4OAc (25 mM). Precipitates were pelleted by centrifugation (16,000 × g, 10 min). The supernatants were dried down under N_2 and resuspended in 450 μL of H_2O with ascorbic acid (30 mM), dipotassium phosphate (50 mM) and 2-mercaptoethanol (0.5%). 25 μL of charcoal-treated rat serum was added to each sample, and the resulting sample was incubated at 37°C for 2 h. Samples were cleaned by Bond Elut PH columns (Agilent Technologies). Columns

were washed with 1 mL of MeOH and conditioned with 1 mL of ascorbic acid buffer (30 mM ascorbic acid, 25 mM NH_4OAc in water). Samples were adjusted to pH 4 using formic acid and were loaded onto the columns. Each column was then washed with 1 mL of the ascorbic acid buffer. Folate species were eluted with 400 μL of 1:1 MeOH:H_2O with 2-mercaptoethanol (0.5% v/v) and NH_4OAc (25 mM). The eluate was dried down under N_2, resuspended in HPLC H_2O, centrifuged (16,000 × g, 5 minutes), and analyzed by LC-MS.

Serum triglycerides were extracted with ethyl acetate. Serum (4 μL) was added to ethyl acetate (100 μL), centrifuged for 10 min at 16,000 x g, and the supernatant collected. The extraction above was repeated once and supernatants combined. The resulting ethyl acetate extract was dried down and redissolved in 1:1:1 MeOH:acetonitrile:2-propanol (200 μL) before analysis by LC-MS. Tissue triglycerides were extracted with 2-propanol. Tissue powder after grinding (5 mg) was added to 2-propanol (200 μL), vortexed for 10 s and then put on dry ice for 10 min. Samples were then centrifuged for 30 min at 16,000 x g and the supernatant used for LC-MS analysis.

LC-MS methods

LC−MS analysis for soluble metabolites was achieved on the Q Exactive PLUS hybrid quadrupole-orbitrap mass spectrometer (Thermo Scientific) coupled with hydrophilic interaction chromatography (HILIC)[24]. To perform the LC separation of ^{13}C-labeled tissue samples, cultured cell samples and all serum samples, an XBridge BEH Amide column (150 mm × 2.1 mm, 2.5 μM particle size, Waters, Milford, MA) was used with a gradient of solvent A (95%:5% H_2O : acetonitrile with 20 mM ammonium acetate, 20 mM ammonium hydroxide, pH 9.4), and solvent B (100% acetonitrile). The gradient was 0 min, 85% B; 2 min, 85% B; 3 min, 80% B; 5 min, 80% B; 6 min, 75% B; 7 min, 75% B; 8 min, 70% B; 9 min, 70% B; 10 min, 50% B; 12 min, 50% B; 13 min, 25% B; 16 min, 25% B; 18 min, 0% B; 23 min, 0% B; 24 min, 85% B; 30 min, 85% B. The flow rate was 150 μL/min; the injection volume was 10 μL; the column temperature was 25 °C. MS full scans were in negative ion mode with a resolution of 140,000 at m/z 200 and scan range of 75 – 1000 m/z. The automatic gain control (AGC) target was 1×10^6.

Deuterium labeled tissue samples and cultured cell samples are analyzed by an almost identical method with modified gradient and a targeted NADP(H) scan. The gradient was: 0 min, 85% B; 2 min, 85% B; 3 min, 60% B; 9 min, 60% B; 9.5 min,35% B; 13 min, 5% B; 15.5 min, 5% B; 16 min, 85% B, 20 mins stop run, and the injection volume was 15 μL. Full scans as above were alternated with targeted scans: m/z 640–765 with a resolution of 35,000 at m/z=200 (AGC target 5×10^5).

To analyze serum acetate, we also used the Q Exactive PLUS hybrid quadrupole-orbitrap mass spectrometer. LC separation was on a reversed phase column (Acquity UPLC BEH C18 column, 2.1 mm x 100 mm, 1.7 5 μm particle size, 130 Å pore size; Waters, Milford, MA) using a gradient of solvent A (water), solvent B (methanol): 0 min, 10% B; 1 min, 10% B; 5 min, 30% B; 11 min, 100% B; 14 min, 100% B; 14.5 min, 10% B; 22 min, 10% B. Flow rate was 200 μL/min and column temperature was 60°C with an injection volume of 10 μL[83]. MS scans were in negative ion mode with a resolution of 15,000 at m/z 200 and scan range of 100–300 m/z. The automatic gain control (AGC) target was 1×10^6.

To analyze folates[84], we again used the Q Exactive PLUS hybrid quadrupole-orbitrap mass spectrometer. LC separation was on a different reversed phase column (Agilent InfinityLab Poroshell 120 Bonus-RP 2.7 μm, 2.1 × 150 mm) with a gradient of solvent A (1% vol of 1M NH_4OAc and 0.1% vol of glacial acetic acid), solvent B (acetonitrile): 4 min, 80% B; 10 min, 2% B; 6 min, 30% B; 11min, 100% B; 15 min, 100% B; 16min, 2% B; 20min 2% B. The flow rate was 200 μL/min and the column temperature was25 °C with an injection volume of 20 μL. MS scans were in negative ion mode with a resolution of 35,000 at m/z 200 and scan range of 350–1000 m/z. The automatic gain control (AGC) target was 1×10^6.

To analyze fatty acids, we used an Exactive orbitrap mass spectrometer. LC separation was via reversed phase-ion-pairing chromatography on a Luna C8 column (150 × 2.0 mm2, 3 μM particle size, 100 Å pore size; Phenomenex) with a gradient of solvent A (10 mM tributylamine + 15 mM acetic acid in 97:3 H2O:MeOH, pH 4.5), solvent B (MeOH): 0 min 80% B; 10 min, 90% B; 11 min, 99% B; 25 min, 99% B; 26 min, 80% B; 30min, 80% B. The flow rate was 250 μL/min and column temperature 25 °C with an injection volume of 5 μL. The MS scans were in negative ion mode with a resolution of 100,000 at m/z 200 and scan range of 120–600. The AGC target was at high dynamic range.

To analyze triglycerides, we used a Q Exactive Plus mass spectrometer coupled to vanquish UHPLC system (ThermoFisher Scientific, San Jose, CA) using positive mode electrospray ionization. The LC separation was achieved on an Agilent Poroshell 120 EC-C18 column (150 × 2.1mm, 2.7 μm particle size) at a flow rate of 150 μL/min. The gradient was 0 min, 25% B; 2 min, 25% B; 4 min, 65% B; 16 min, 100 %B; 20 min, 100% B; 21 min, 25% B; 27 min, 25% B. Solvent A is 1 mM ammonium acetate + 0.2% acetic acid in water:methanol (90:10). Solvent B is 1mM ammonium acetate +0.2% acetic acid in methanol:2-propanol (2:98).

All data from labeling experiments were analyzed by El-MAVEN[85] and subjected to natural abundance correction[86].

GC-MS for plasma D_2O measurement

Plasma D_2O was measured by headspace GC-MS[87]. 10 μL of plasma or D_2O standard sample was mixed with 5 μL 10 N sodium hydroxide and 10 μL acetone in a sealed 20 mL screw-top GC headspace vial (Agilent 5188–2573) at room temperature and the base-catalyzed hydrogen (deuterium) exchange reaction between water/plasma water and acetone was allowed for 6 hours. D_2O standard samples were prepared by a serial two-third dilution of a solution of 30% D_2O down to 0.0135% D_2O in water. 25 μL of each sample from headspace was then injected in an Agilent GC/MS system (Agilent 7000D MS coupled with 7890B GC system) with a 2 min isothermal run using a J&W HP-5ms GC column (Agilent 19091s-433, 30 m, 0.25 mm, 0.25 m) in split mode (10:1 split ratio). GC-MS parameters were oven temperature 170°C, inlet temperature: 250°C, source temperature: 270°C, MS1 Quad temperature 150°C, Aux-2 temperature: 250°C, He carrier flow: 1 mL/min. Selected-ion monitoring was carried out for m/z 58–62. The ratio of integrated area of m/z 60 vs 59 from deuterated/unlabeled acetone (eluting at ~ 1.4 min) was determined.

Data analysis

1. Quantification of *de novo* lipogenesis flux with D_2O

1) Long-term steady-state analysis with oral D_2O: D_2O labels lipogenic fat both directly and via NADPH. Accordingly, a double binomial distribution model was used to calculate the palmitate labeling pattern based on experimentally measured D_2O and NADPH labeling[24]. Fractional D_2O enrichment *in vivo* $\boldsymbol{p_1}$ was determined based on labeling of soluble metabolites pairs (malate-fumarate; glutamate-ketoglutarate). NADPH active-H labeling $\boldsymbol{p_2}$ was calculated based on the NADPH-$NADP^+$ pair (Supplementary Figure 1):

$$\begin{bmatrix} M+0 & 0 \\ M+1 & M+0 \\ \vdots & M+1 \\ M+i & \vdots \\ 0 & M+i \end{bmatrix} \times \begin{bmatrix} 1-p \\ p \end{bmatrix} = \begin{bmatrix} M+0 \\ M+1 \\ \vdots \\ M+i \\ M+i+1 \end{bmatrix} \quad (1)$$

In the above equation, the matrix on the left-hand side contains the experimentally measured mass isotope distribution for the compound on the left-hand side in the equations in the above schematic (the same compound's mass isotope distribution is in both columns, offset as indicated). The matrix on the right-hand side contains the experimentally measured mass isotope distribution for the compound on the right-hand side in the above equations. The value of $\boldsymbol{p}$ is determined by solving the resulting linear equations. Values of $\boldsymbol{p_1}$ are the average of $\boldsymbol{p}$ determined using fumarate-malate and α-ketoglutarate-glutamate; $\boldsymbol{p_2}$ is solely determined by NADP-NADPH. This method gives the same serum D_2O enrichment as standard GC-MS measurements (Extended Data Fig. 1f).

For the infusion of other deuterium tracers ([1-^{2}H]glucose and [2,3,3-^{2}H]-serine), NADPH active-H labeling is also calculated by *eq* 1.

Synthesis of one palmitate molecule (C16:0) requires 7 repeated reactions that incorporate 7 hydrogens from water and 14 hydrogens from NADPH. The expected **(*E*)** number of deuterium in one palmitate is

$$E = 7 \times p_1 + 14 \times p_2 \quad (2)$$

Let $\boldsymbol{M_i}$ be the fraction of palmitate containing $\boldsymbol{i}$ deuterium atoms (i.e. measured fraction at mass $M + i$ after correcting for natural isotope abundance). Then $\boldsymbol{D}$ is the average measured number of deuterium accumulated at steady state per palmitate

$$D = \sum_{i=0} M_i \times i \quad (3)$$

Define:

$\boldsymbol{F}$ = *de novo* lipogenic fatty acid (palmitate) amount at steady state

$\boldsymbol{C}$ = total fatty acid (palmitate) amount at steady state

F/C = fraction palmitate synthesized *de novo*

The total deuterium assimilated is given by both (i) total fatty acid amount (**C**) x measured average deuterium per fatty acid (**D**) and (ii) newly synthesized fatty acid amount (to be determined) x expected deuterium per newly synthesized fatty acid (**E**):

$$\mathbf{C} \times \mathbf{D} = \mathbf{F} \times \mathbf{E}$$

$$\textbf{Fractional newly synthesized fatty acid at steady state} = \frac{F}{C} = \frac{D}{\mathbf{E}} \quad (4)$$

2) Kinetic analysis of *de novo* lipogenesis with D_2O infusion: For the 12 h infusion experiments, D_2O in serum is not at steady state and accordingly a slightly more complex calculation is required. D_2O increases linearly with infusion time (Sup. Fig. 1g). The final serum D_2O enrichment **(p_1)** can thus be written as a linear function of time:

$$p_1 = \mathbf{t} \times k_1 \quad (5)$$

Due to the rapid H-D exchange flux, tissue NADPH labeling reaches equilibrium with serum water labeling quickly, and therefore tissue NADPH will also rise linearly over time:

$$p_2 = \mathbf{t} \times k_2 \quad (6)$$

where:

$$k_2/k_1 = H_{exchange} \quad (7)$$

The expected deuterium per palmitate ***(E)*** will be:

$$E = 7 \times p_1 + 14 \times p_2 = 7 \times k_1 \times t + 14 \times k_2 \times t \quad (8)$$

Define f (gram/hour) as the average *de novo* lipogenesis flux of palmitate per hour. For an infusion of duration t hours, the total deuterium amount incorporated into newly synthesized palmitate is:

$$\int f \times E \, dt = D \times C \quad (9)$$

$$f \times \left(\frac{7}{2} k_1 \times t^2 + 7k_2 + t^2\right) = D \times C \quad (10)$$

$$\frac{f}{C} = \frac{D}{(3.5k_1 + 7k_2) \times t^2} \quad (11)$$

Newly synthesized palmitate ***(F)*** in t = 12 h is given by:

$$\frac{F}{C} = \frac{12 \times f}{C} = \frac{D}{(3.5k_1 + 7k_2 \times 12)} \quad (12)$$

2. Quantification of direct carbon contribution from circulating substrates— The direct carbon sources for lipogenesis can be analyzed similarly to the direct circulating nutrient contribution to TCA[26]. Since F_{circ}[26] of glucose, lactate and acetate are high, their labeling in serum reaches steady state within ~1 h of infusion. Saponified fatty acid labeling, however, does not reach steady state over 12 h. So, an extra factor of newly synthesized fat ($\frac{F}{C}$ from *eq* 12) needs to be included.

Here, we define $f_{Pal \leftarrow Met}$ as the carbon flux directly coming from a given circulating metabolite to palmitate. By direct, we mean that the circulating metabolite is taken up into the lipogenic tissue (liver or adipose) and converted within the tissue to acetyl-CoA that is used for fat synthesis. This contrasts with circulating metabolites that are converted into a different circulating lipogenic precursor before entering the lipogenic tissue to support fat synthesis. Here, we assessed six potential lipogenic substrates: glucose (glc), lactate (lac), acetate (act), glutamine (gln), alanine (ala) and citrate (cit).

Define $L_{Met2 \leftarrow Met1}$ as the average pseudo-steady-state ^{13}C-labeling fraction per carbon in metabolite_2 after infusion of U-^{13}C- labeled metabolite_1 as the tracer. To calculate enrichment, let N_i be the fraction of the metabolite containing i ^{13}C atoms (after natural isotope correction) and n the total carbon number of the metabolite:

$$L_{Met} = \frac{\sum_{i=0-n} N_i \times i}{n} \quad (13)$$

$$L_{Met2 \leftarrow Met1} = \frac{L_{Met2}}{L_{Met1}} \quad (14)$$

Define the pre-steady-state ^{13}C-labeling measured in saponified palmitate as $L_{pal \leftarrow Met1\_12h}$. The expected pseudo-steady-state palmitate labeling is then given by dividing by the fraction of newly synthesized palmitate over the 12 h:

$$L_{pal \leftarrow Met1} = \frac{L_{pal \leftarrow Met1\_12h}}{F/C} \quad (15)$$

Liver is fed by 22% systemic arterial blood and 78% portal vein blood[88]; brown adipose tissue is fed by arterial blood[83]. Artery labeling was calculated based on tail vein blood labeling[26], and portal vein labeling was directly measured. We can then solve the direct carbon flux to *de novo* lipogenesis in liver and brown adipose tissue with the following equation:

$$\begin{bmatrix} 1 & L_{lac\leftarrow glc} & L_{act\leftarrow glc} & L_{gln\leftarrow glc} & L_{ala\leftarrow glc} & L_{cit\leftarrow glc} \\ L_{glc\leftarrow lac} & 1 & L_{act\leftarrow lac} & L_{gln\leftarrow lac} & L_{ala\leftarrow lac} & L_{cit\leftarrow lac} \\ L_{glc\leftarrow lac} & L_{lac\leftarrow act} & 1 & L_{gln\leftarrow act} & L_{ala\leftarrow act} & L_{cit\leftarrow act} \\ L_{glc\leftarrow gln} & L_{lac\leftarrow gln} & L_{act\leftarrow gln} & 1 & L_{ala\leftarrow gln} & L_{cit\leftarrow gln} \\ L_{glc\leftarrow ala} & L_{lac\leftarrow ala} & L_{act\leftarrow ala} & L_{gln\leftarrow ala} & 1 & L_{cit\leftarrow ala} \\ L_{glc\leftarrow cit} & L_{lac\leftarrow cit} & L_{act\leftarrow cit} & L_{gln\leftarrow cit} & L_{ala\leftarrow cit} & 1 \end{bmatrix} \times \begin{bmatrix} f_{pal\leftarrow glc} \\ f_{pal\leftarrow lac} \\ f_{pal\leftarrow act} \\ f_{pal\leftarrow gln} \\ f_{pal\leftarrow ala} \\ f_{pal\leftarrow cit} \end{bmatrix} = \begin{bmatrix} L_{pal\leftarrow glc} \\ L_{pal\leftarrow lac} \\ L_{pal\leftarrow act} \\ L_{pal\leftarrow gln} \\ L_{pal\leftarrow ala} \\ L_{pal\leftarrow cit} \end{bmatrix} \quad (16)$$

3. Quantification of fractional NADPH contribution from different production pathways—Deuterium-labeled metabolite tracers label NADPH's active-H[24]. Active-H labeling in NADPH was determined from the isotopic pattern of NADPH relative to $NADP^+$ (*eq* 1). The fraction of NADPH coming from different pathways was calculated as described previously[24]:

$$\begin{aligned} &\textit{Fractional NADPH contribution} \\ &= \frac{Active-H\ labeling \times (\#\ \ NADPH\ made\ by\ pathway)}{Substrate\ labeling \times (1-H_{exchange})} \end{aligned} \quad (17)$$

NADPH made by pathway is 2 for the oxidative PPP and 1 otherwise. $H_{exchange}$ refers to the fraction of NADPH undergoing H-D exchange with water. Experimental measurements of NADPH and fat labeling after D_2O infusion gave out $H_{exchange}$ in liver and brown adipose (*eq* 7; Sup. Fig. 4f–g). Tissue glucose-6-phosphate labeling was used as substrate labeling for calculating the oxPPP contribution; tissue serine M+2 and M+3 labeling (summed) was used as substrate labeling for calculating the serine contribution. No correction was made for the deuterium kinetic isotope effect.

Data and code availability

Raw data are provided in source data files. El-MAVEN v12 and natural abundance correction software accucor are available online on Github.

Statistics

All statistics are done by two-sided unpaired Mann-Whitney test. Data distribution was assumed to be normal but this was not formally tested.

Extended Data

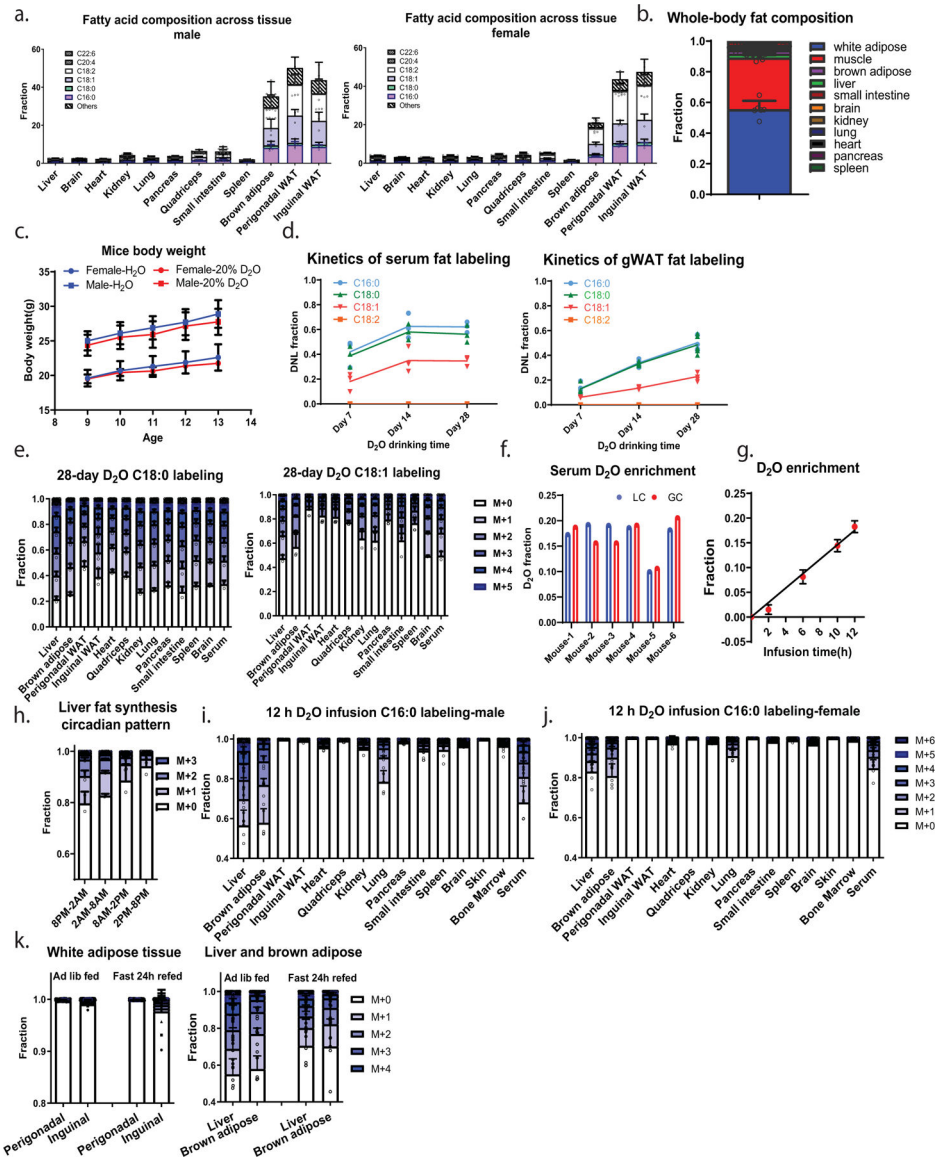

Extended Data Figure 1. Fatty acid composition and D_2O labeling across tissues and time

a. Fraction of tissue weight that is fat, and composition of those fatty acids in male and female mice.

b. Fat is stored in white adipose tissue, and to a lesser extent in muscle. Muscle values are calculated assuming quadriceps is representative of whole-body muscle.

c. Body weight of mice drinking 20% D_2O for 4 weeks (control data are from Jackson lab website).

d. Fatty acid labeling from D_2O reaches steady-state more quickly in serum than in white adipose, while different fatty acid species reach steady-state at a similar rate.

e. C18:0 and oleate (C18:1) labeling pattern across tissues after 4 weeks of D_2O drinking.

f. Serum D_2O enrichment measured by LC-MS and GC-MS.

g. Labeling of serum D_2O increases linearly over time for the 12 h of infusion.

h. Circadian pattern of liver fat synthesis based on 6 h D_2O infusions.
i. C16:0 labeling pattern across tissues after 12 h fed-state D_2O infusion in male mice.
j. As is (j), for female mice.
k. C16:0 labeling in white adipose tissue, liver, and brown adipose tissue from 12 h refed D_2O infusion after 24 h fast.
Mean ± s.d., n=3 of both genders for fat composition analysis; n=4 male mice for steady-state analysis and body composition analysis; n=4 of both genders for bodyweight measurement; n=2 male mice for 6 h D_2O infusions; n=5 of both genders for 12 h D_2O infusion; n=5 males in each group for the fasted-refed experiments.

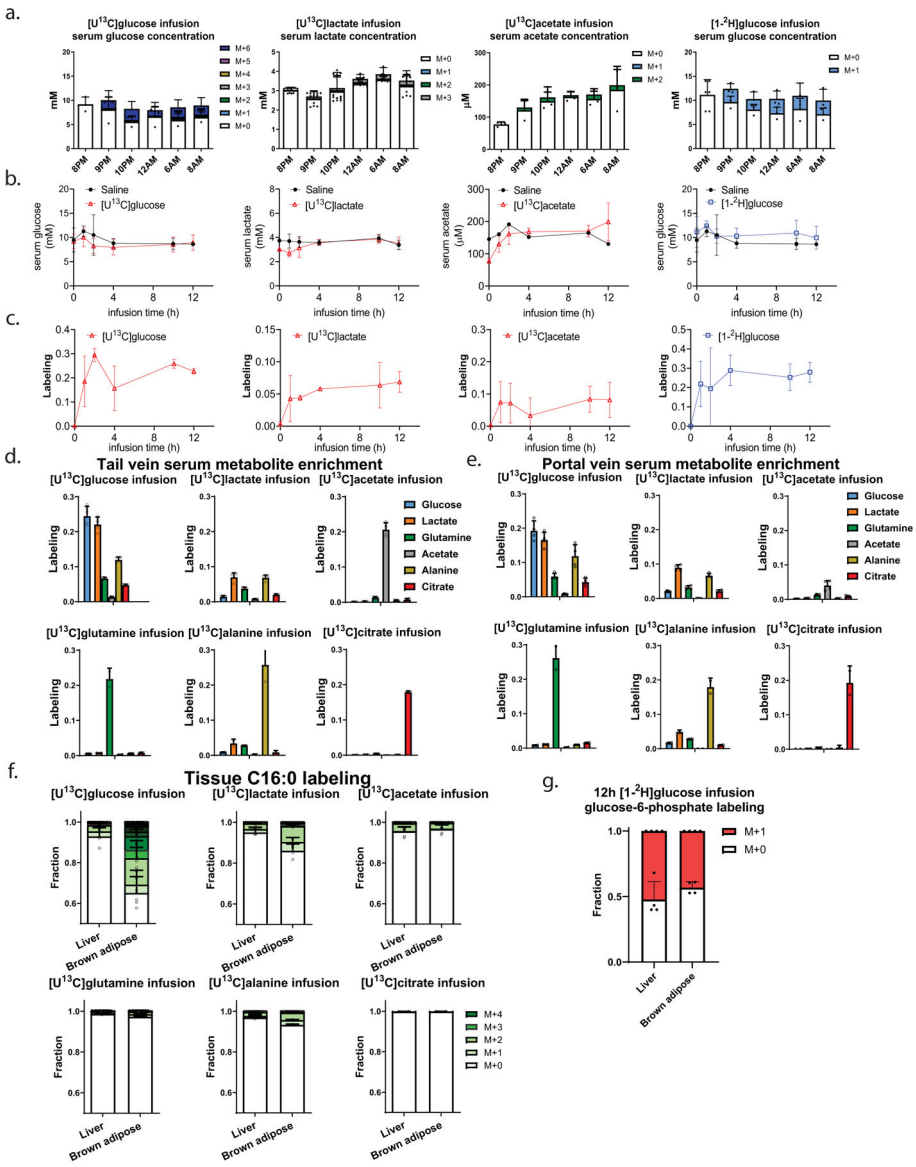

Extended Data Figure 2. Circulating metabolite levels and labeling and tissue saponified fat labeling from carbon tracers and [1-^{2}H]glucose

a. Circulating concentrations of unlabeled and labeled forms during the indicated tracer infusions.

b. Corresponding total concentrations.

c. Corresponding average carbon atom labeling (for the 13C tracers) or labeled fraction (for the [1-^{2}H]glucose tracer).

d. Tail vein serum circulating metabolite average carbon atom labeling from different infused ^{13}C tracers (each sampled at end of 12 h infusion).

e. As in (d), from portal vein.

f. Corresponding C16:0 labeling in liver and brown adipose.

g. Glucose-6-phosphate labeling from 12 h [1-^{2}H]glucose infusion in liver and brown adipose tissue.

All data are mean ± s.d. For time-point samples, [U-^{13}C]glucose (n=3), lactate (n=3), acetate (n=3), [1-^{2}H]glucose (n=4), saline (n=2); for other samples [U-^{13}C]glucose (n=4), lactate (n=4), glutamine (n=2), acetate (n=4), alanine (n=2) citrate (n=2) and [1-^{2}H]glucose (n=4). All mice are males. For female data, see Sup. 6.

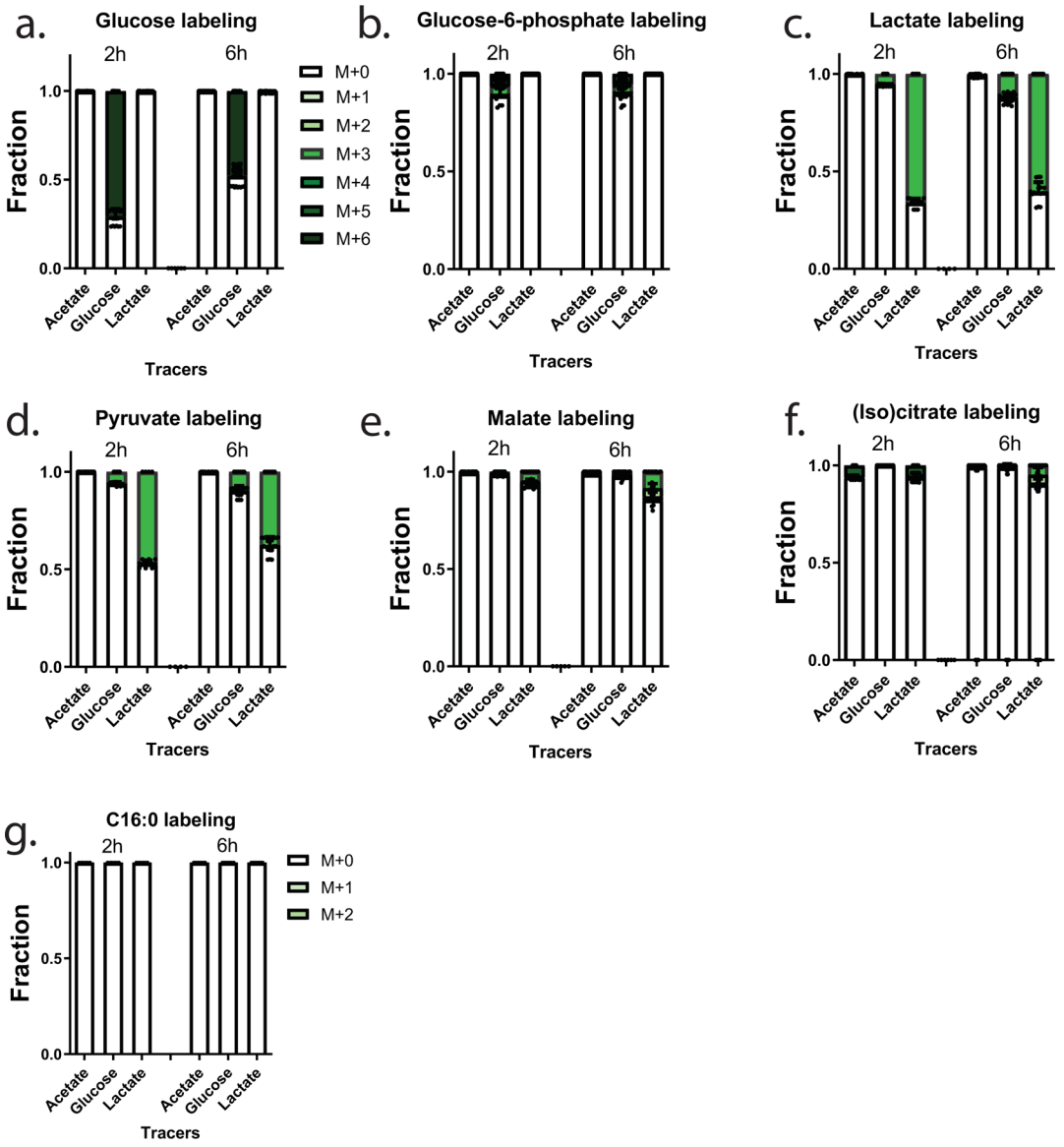

Extended Data Figure 3. Carbon tracing in liver slices

a-g. Labeling of the indicated metabolites in liver slices after 2 h or 6 h incubation in Krebs-Ringer buffer containing glucose, lactate, and acetate, with the indicated metabolite provided in [U^{13}C]-labeled form.

Data are mean ± s.d.; n=2 mice for 2 h experiments; n=3 mice for 6 h experiments, 2 technical replicates (independent tissue slices) from each mouse liver. All mice are males.

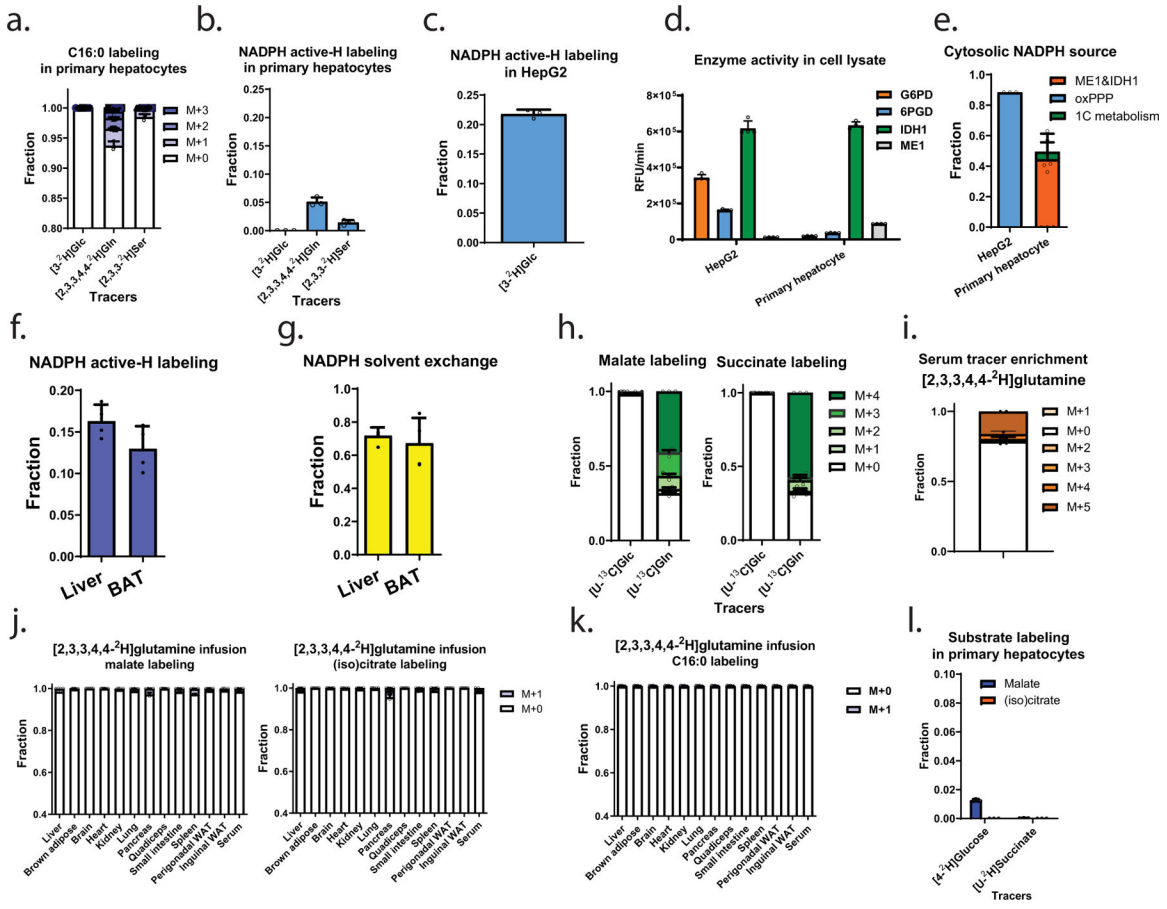

Extended Data Figure 4. Hepatocytes are deficient in the oxPPP, and [2,3,3,4,4-^{2}H]glutamine tracer works to probe malic enzyme and IDH flux in cultured hepatocytes but not *in vivo*

a. C16:0 labeling over 6 h from different tracers in primary hepatocytes.

b. NADPH active-H labeling over 2.5 h from different tracers in primary hepatocytes.

c. NADPH active-H measurement over 2.5 h from [3-^{2}H]glucose in HepG2 cells.

d. Enzymatic activity of G6PD, 6PGD, IDH1 and ME1 in lysates from HepG2 cells and primary murine hepatocytes.

e. Hydride sources supporting *de novo* lipogenesis in HepG2 cells and primary hepatocytes, correcting for substrate labeling and H-D exchange between NADPH and water.

f. NADHP active hydrogen labeling from 12 h D_2O infusion in liver and brown adipose

g. The fraction of active hydrogen on NADPH that undergoes solvent exchange with water calculated from 12 h D_2O infusion in liver and brown adipose.

h. Glutamine is the dominant TCA substrate in cultured primary hepatocytes.

i. Serum tracer labeling at the end of 12 h [2,3,3,4,4-^{2}H]glutamine infusion.

j. Minimal malate and (iso)citrate labeling from [2,3,3,4,4-^{2}H]glutamine infusion across tissues *in vivo*.

k. C16:0 labeling from [2,3,3,4,4-^{2}H]glutamine infusion across tissues.

l. Minimal malate and (iso)citrate labeling from [4-^{2}H]glucose and [U-^{2}H]succinate in cultured primary hepatocytes.

All data are mean ± s.d., n=4 for solvent exchange measurement, n=2 for [2,3,3,4,4-^{2}H]glutamine infusion, all mice are males, n=3 biological replicates for all cell culture experiments.

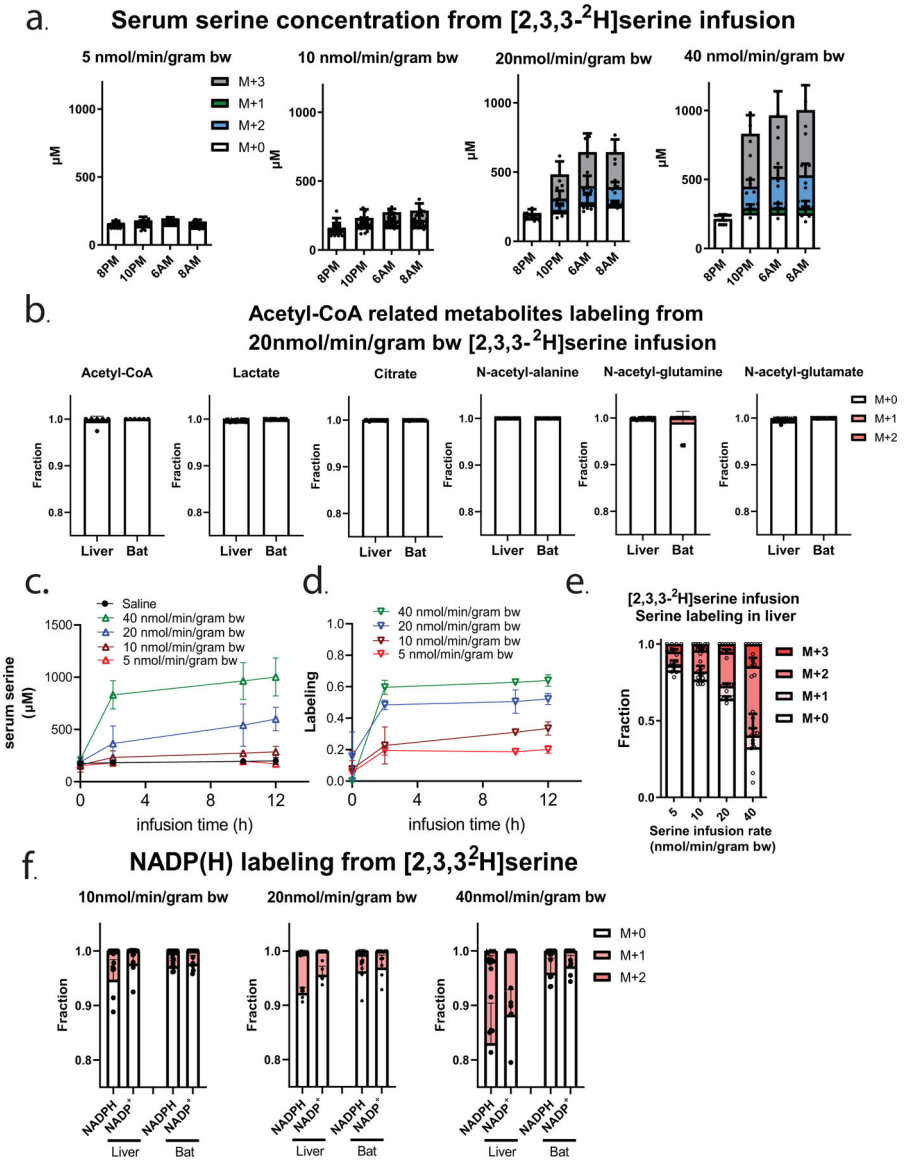

Extended Data Figure 5. Serine's hydride contribution to liver fat across 8-fold range of [2,3,3-^{2}H]serine infusion rates

a. Circulating serine labeling during [2,3,3-^{2}H]serine infusion at different rates, ranging from minimally to highly perturbative.

b. Lack of labeling in liver acetyl-CoA and related metabolites from 12 h [2,3,3-^{2}H]serine infusion (20 nmol/min/gram body weight).

c. Circulating serine concentrations during [2,3,3-^{2}H]serine infusion at different rates, ranging from minimally to highly perturbative (sum of unlabeled and labeled).

d. Corresponding serine labeling (average atom labeling of serine side chain hydrogens).

e. Liver serine labeling after 12 h [2,3,3-^{2}H]serine infusion.

f. Corresponding liver and brown adipose tissue NADP(H) labeling.

All data are mean ± s.d., For time point experiments n=3 for each tracer and n=2 for saline. For C16:0, NADPH, acetyl-CoA, and related metabolite labeling, n=4 for 5 nmol/min/gram bodyweight and n=6 for 10, 20 and 40 nmol/min/gram bodyweight of [2,3,3-^{2}H]serine infusion. All mice are males.

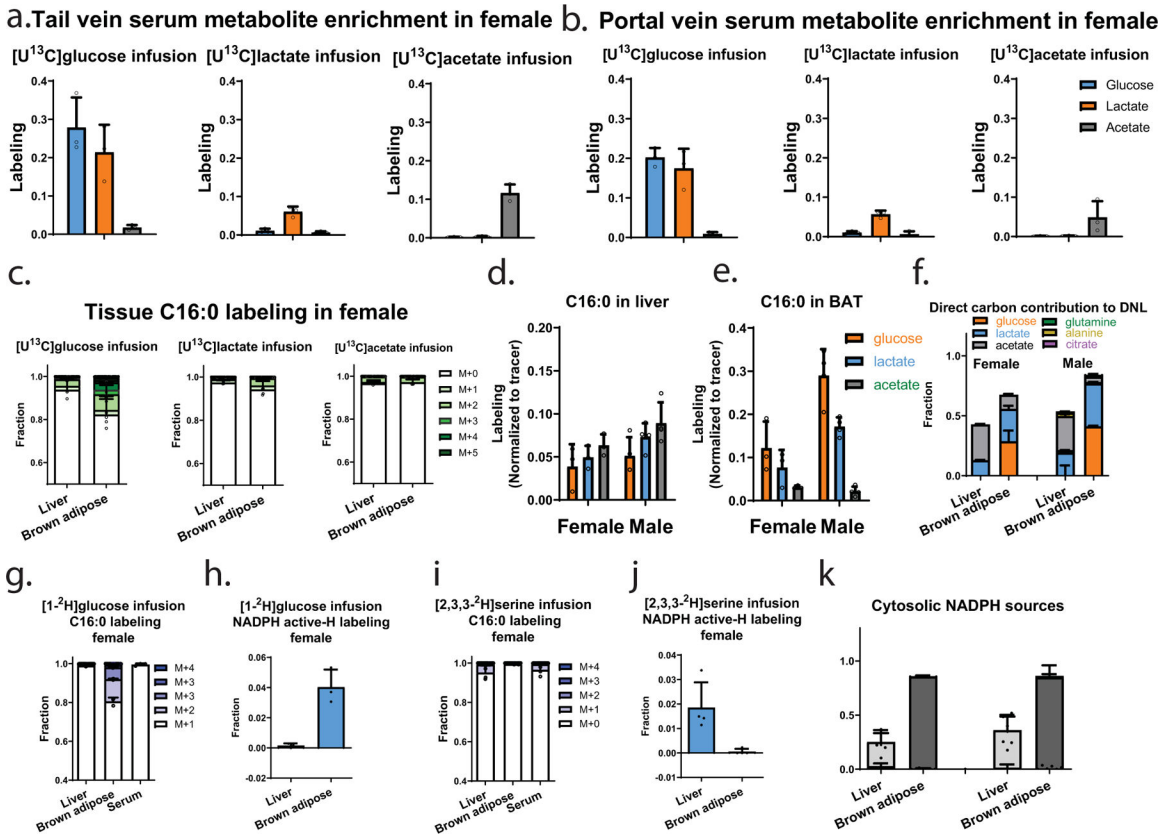

Extended Data Figure 6. Carbon and hydrogen inputs to lipogenesis are consistent across female and male mice

a. Tail vein serum circulating metabolite average carbon atom labeling from different infused ^{13}C tracers (each after 12 h infusion) in female mice.

b. Corresponding portal vein serum circulating metabolite labeling in female mice.

c. Corresponding C16:0 labeling in liver and brown adipose in female mice.

d. Fractional enrichment of liver and brown adipose tissue C16:0 in female mice following 12 h infusion of [U-^{13}C]-labeled glucose (n=3), lactate (n=3), acetate (n=3). Male data are the same as Fig. 2b. Labeling is normalized to circulating tracer enrichment. Brown adipose is fueled by systemic blood (approximated by tail vein sampling) and liver is fueled by 78% portal vein blood and 22% systemic blood.

e. As is (d), for brown adipose C16:0.

f. Carbon sources supporting *de novo* lipogenesis in liver and brown adipose in female and male mice, based on direct contributions to C16:0, calculated based on data in (d) and (e). Male data are the same as Fig.2d.

g. C16:0 labeling in liver, brown adipose and serum following 12 h [1-^{2}H]glucose infusion (125 nmol/min/gram body weight) in female mice (n=3).
h. NADPH active-H measurement in liver and brown adipose from 12 h [1-^{2}H]glucose infusion (125 nmol/min/gram bw)in female mice (n=4).
i. As is (g), for 12 h [2,3,3-^{2}H]serine infusion (20 nmol/min/gram bw).
j. As is (h), for 12 h [2,3,3-^{2}H]serine infusion (20 nmol/min/gram bw).
k. Hydride sources supporting *de novo* lipogenesis in liver and brown adipose in female and male mice, correcting for substrate labeling and H-D exchange between NADPH and water. Calculated based on tracer data in (b) and (d) and D_2O exchange data in Sup.4i. Male data are the same in Fig. 3g.
Data in f are mean ± s.e.m.; other data are mean ± s.d.

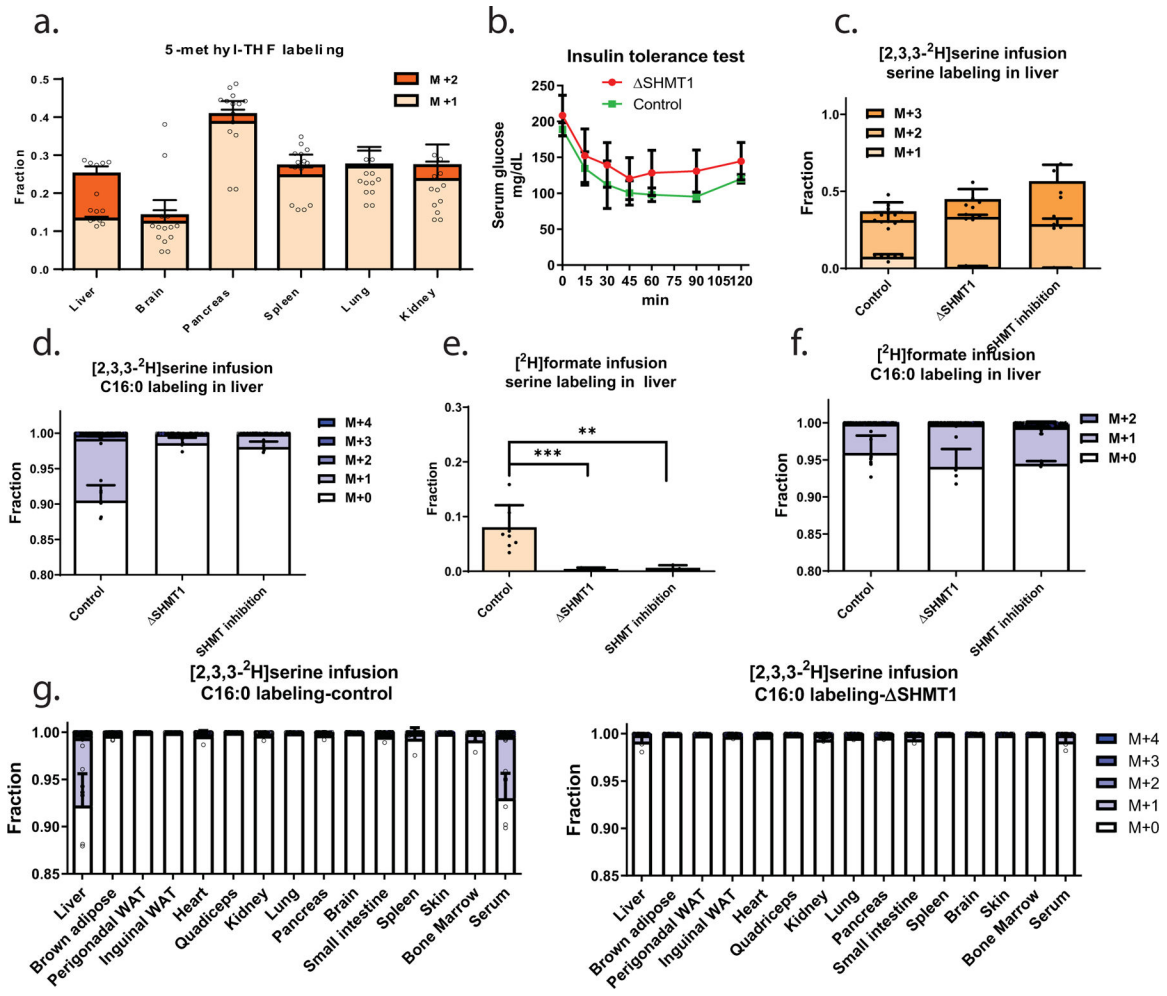

Extended Data Figure 7. Cytosolic serine catabolism in the liver is blunted by SHMT knockout or inhibition.

a. 5-methyl-THF labeling from 12 h [2,3,3-^{2}H]serine (20 nmol/min/gram body weight). M+2 labeling reflects cytosolic serine catabolism. M+1 labeling reflects the combination of mitochondrial serine catabolism and reversible flux through MTHFD1.
b. Glucose levels after insulin tolerance test in control and whole-body ΔSHMT1 mice.

c. Serine labeling in liver from 12 h [2,3,3-^{2}H]serine infusion (20 nmol/min/gram bw) in control, whole-body ΔSHMT1 mice, and mice treated with the dual SHMT1/2 inhibitor SHIN2 (3.33 mg/kg/h i.v. infusion).

d. C16:0 labeling in liver from 12 h [2,3,3-^{2}H]serine infusion (20 nmol/min/gram bw).

e. As is (c), for [^{2}H]formate infusion. (control vs. ΔSHMT1, p=0.0010; control vs. SHIN2 treatment, p=0.0091).

f. As is (d), for [^{2}H]formate infusion.

g. C16:0 labeling across tissues following 12 h [2,3,3–2H]serine infusion (20 nmol/min/gram body weight) in control and ΔSHMT1 mice.

Mean ± s.d. For insulin tolerance tests, n=12 for SHMT1 knock out mice, n=4 for littermate wild type controls. For serine and formate infusions, n=6 for control, n=4 for ΔSHMT1, n=4 for SHIN2 treatment. For [2,3,3-^{2}H]serine infusion in ΔSHMT1 mice, n=4 for liver, bat, brain bone marrow, serum, and skin; n=3 for other tissues; control mice data are the same as Fig.3e. For D_2O tracing experiments, n=10 in each group. *p<0.05; **p<0.01; ***p<0.005 by unpaired Mann-Whitney test. All mice are males.

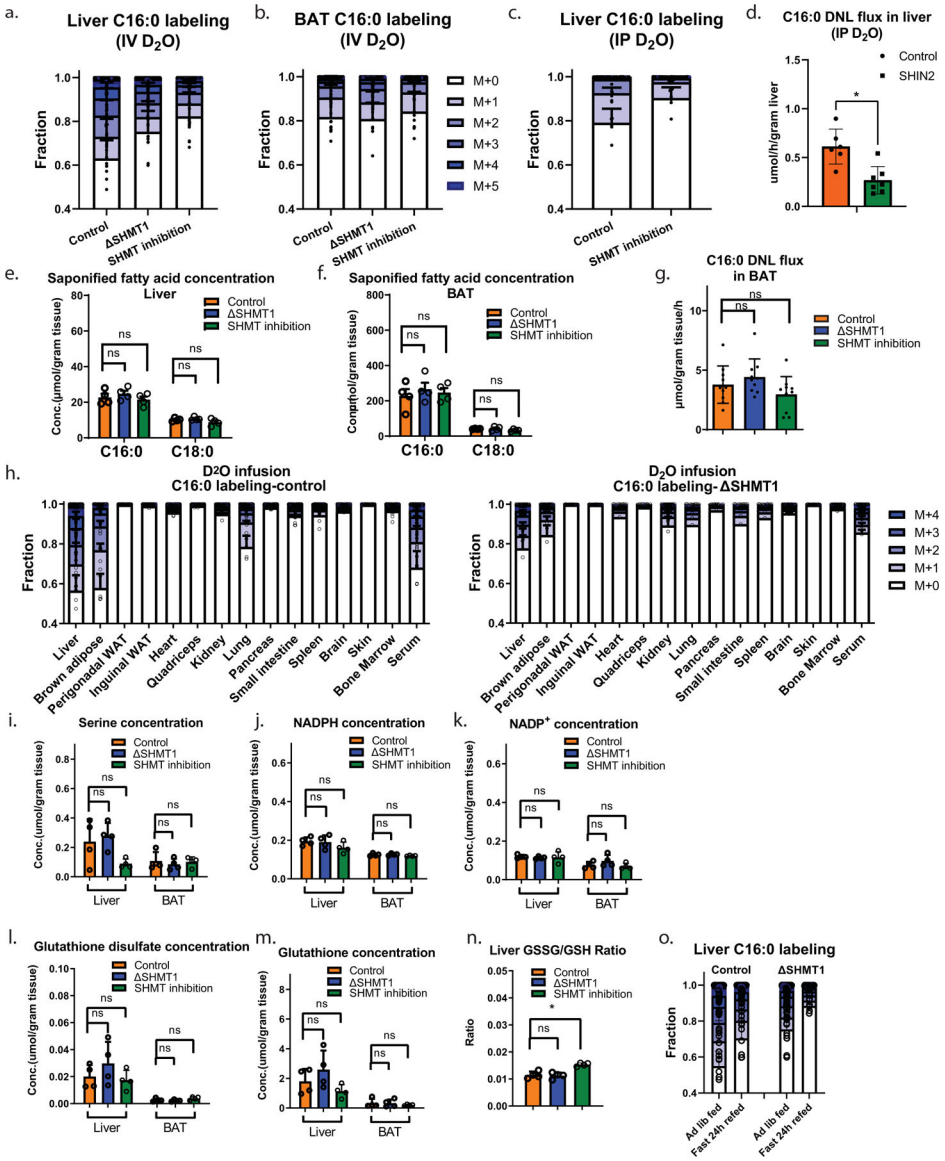

Extended Data Figure 8. Concentrations and labeling of saponified fatty acids and soluble metabolites in wild type, ΔSHMT1, and SHMT inhibitor-treated mice (3.33 mg/kg/h i.v. infusion of SHIN2 for 12 h)

a. Saponified C16:0 labeling pattern in liver following 12 h D_2O infusion to control, ΔSHMT1, and SHIN2-treated mice (SHIN2 infused simultaneous with the D_2O infusion).

b. As is (a), for brown adipose.

c. Saponified C16:0 labeling pattern in liver following 12 h IP D_2O to control and SHIN2-treated mice (SHIN2 infused simultaneous).

d. C16:0 lipogenesis flux in liver overnight, as measured by IP D_2O injection. (control vs. SHIN2 treatment, p=0.0047)

e. C16:0 and C18:0 concentration in liver of control, ΔSHMT1, and SHIN2-treated mice (control vs. ΔSHMT1, p=0.48 for C16:0, p= 0.88 for C18:0; control vs. inhibitor, p=0.48 for C16:0, p= 0.34 for C18:0).

f. As is (a), for brown adipose tissue (control vs. ΔSHMT1, p=0.68 for C16:0, p=0.99 for C18:0; control vs. SHIN2 treatment, p=0.99 for C16:0, p=0.11 for C18:1).
g. C16:0 lipogenesis flux in brown adipose tissue overnight, as measured by 12 h D_2O infusion (control vs. ΔSHMT1, p=0.32; control vs. SHIN2 treatment, p=0.28).
h. C16:0 labeling across tissues following 12 h D_2O infusion in control and ΔSHMT1 mice.
i. Serine concentration in liver and brown adipose tissue of control, ΔSHMT1, and SHIN2-treated mice (control vs. ΔSHMT1, p=0.99 for liver, p=0.99 for BAT; control vs. SHIN2 treatment, p=0.34 for liver, p=0.34 for BAT).
j. As is (c), for NADPH (control vs. ΔSHMT1, p=0.99 for liver, p=0.88 for BAT; control vs. SHIN2 treatment, p=0.11 for liver, p=0.20 for BAT).
k. As is (c), for $NADP^+$ (control vs. ΔSHMT1, p=0.34 for liver, p=0.34 for BAT; control vs. SHIN2 treatment, p=0.68 for liver, p=0.48 for BAT).
l. As is (c), for glutathione (control vs. ΔSHMT1, p=0.34 for liver, p=0.68 for BAT; control vs. SHIN2 treatment, p=0.48 for liver, p=0.99 for BAT).
m. As is (c), for glutathione disulfide (control vs. ΔSHMT1, p=0.34 for liver, p=0.88 for BAT; control vs. SHIN2 treatment, p=0.88 for liver, p=0.14 for BAT).
n. Liver glutathione disulfide vs. reduced glutathione ratio in control, ΔSHMT1, and SHIN2-treated mice (control vs. ΔSHMT1, p=0.99; control vs. SHIN2 treatment, p=0.029).
o. Liver C16:0 labeling pattern after 12 h D_2O infusion during ad lib feeding and in mice subjected to 24 h fasting followed by refeeding (control data is the same as Sup.1l; ΔSHMT1 ad lib fed data are the same as Sup.7f).
Mean± s.d, n=4 for control, ΔSHMT1, and SHIN2-treated mice. For refeeding experiment, n=3 for ΔSHMT1 refed. For D_2O infusion in ΔSHMT1 mice, n=2 for liver, bat, white adipose, lung, brain, bone marrow, serum, and skin; n=1 for other tissues; control mice data are the same as Sup.1i. *p<0.05 by unpaired Mann-Whitney test. All mice are males.

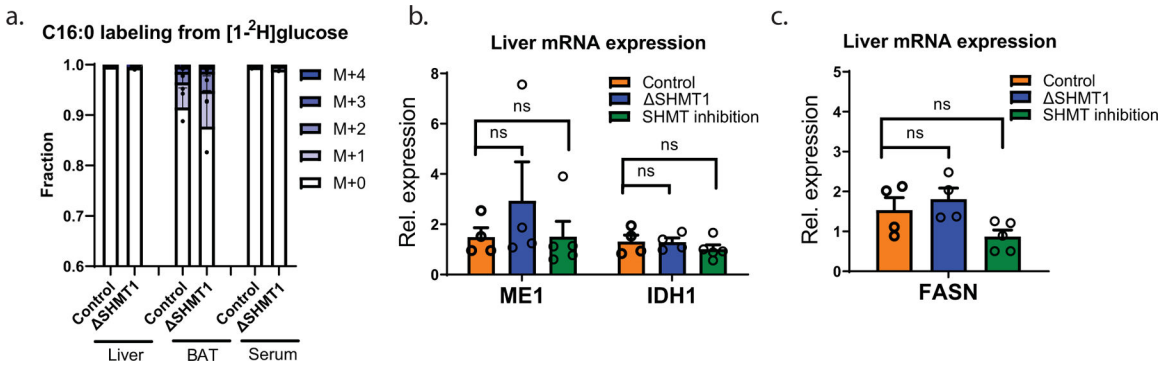

Extended Data Figure 9. Knockout of SHMT1 does not induce alternative NADPH producing enzymes.

a. C16:0 labeling from [1-^{2}H]glucose in liver, brown adipose tissue, and serum in control and ΔSHMT1 mice.

b. Relative mRNA expression level of Malic Enzyme 1 (ME1) and Isocitrate dehydrogenase 1 (IDH1) in liver of control, ΔSHMT1, and 12 h SHIN2 treated mice (3.33 mg/kg/h i.v. infusion) (control vs. ΔSHMT1, p=0.48 for ME1, p=0.88 for IDH1; control vs. inhibitor, p=0.73 for ME1, p=0.56 for IDH1.)

c. Relative mRNA expression level of fatty acid synthase (FASN) in liver of control, ΔSHMT1, and 12 h SHIN2 treated mice (3.33 mg/kg/h i.v. infusion) (control vs. ΔSHMT1, p=0.48 for control vs. inhibitor, p=0.26.)

Mean± s.d. N=2 mice in each group for [1-^{2}H]glucose infusion. For qPCR, n=4 for control, n=4 for ΔSHMT1, n=5 for SHIN2 treatment, p-values from unpaired Mann-Whitney test. All mice are males.

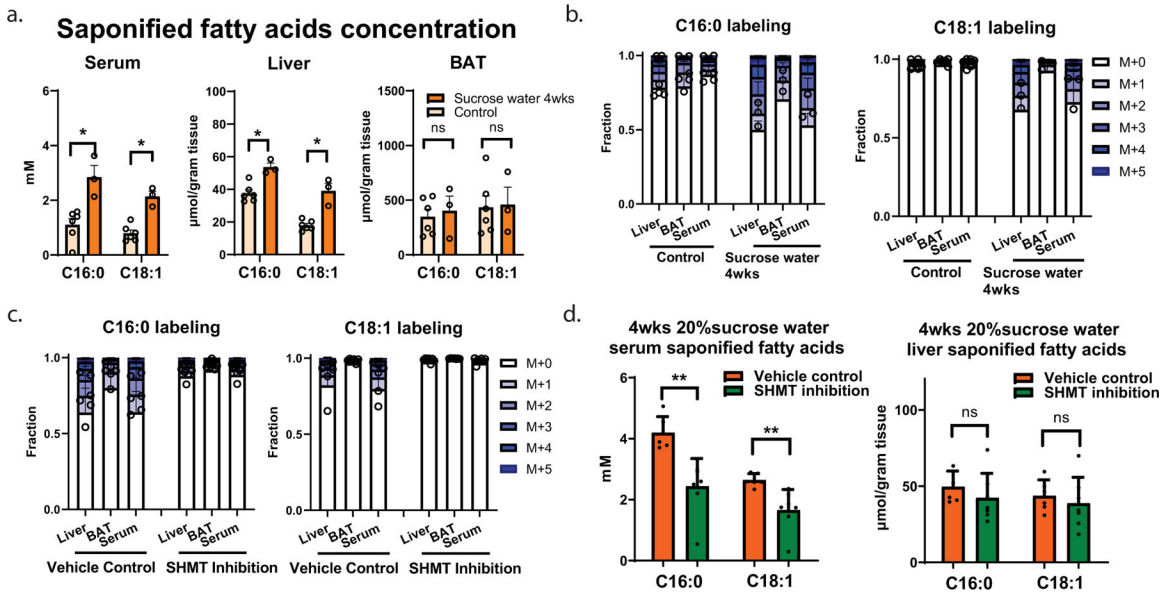

Extended Data Figure 10. SHMT inhibition reduced sucrose-water induced hepatic lipogenesis increase

a. Saponified C16:0 and C18:1 concentration of serum, liver, and BAT in control and 4 weeks 20% sucrose water drinking mice (control vs. sucrose water drinking, serum p=0.024 for C16:0, p= 0.024 for C18:1; liver p=0.024 for C16:0, p= 0.024 for C18:1; BAT p=0.90 for C16:0, p= 0.99 for C18:1.).

b. C16:0 and C18:1 labeling fraction in liver, brown adipose tissue, and serum from fed state 12 h D_2O infusion of control and 4 weeks 20% sucrose water drinking mice.

c. Saponified C16:0 and C18:1 labeling in liver, brown adipose tissue, and serum with or without SHIN2 treatment.

d. Overall serum levels of fatty aicds instead of labeling with or without SHIN2 treatment (control vs. SHIN2 treatment, p=0.0022 for C16:0; p= 0.0043 for C18:1).

e. As is (g), for liver (control vs. SHIN2 treatment, p=0.23 for C16:0, p= 0.44 for C18:1).

Mean± s.d. For experiments comparing control to sucrose water drinking, n=6 for control, n=3 for 4-week sucrose water drinking. For experiments comparing vehicle to SHIN2 treatment, n=6 for control and n=7 for SHIN2. *p<0.05; **p<0.01; ***p<0.005 by unpaired Mann-Whitney test. All mice are males.

Supplementary Material

Refer to Web version on PubMed Central for supplementary material.

Acknowledgements

This work was supported by NIH Pioneer award 1DP1DK113643 and Pfizer, Inc. T.T. is supported by NIH fellowship 1F32DK118856. L.Y. was supported by a postdoctoral fellowship from the New Jersey Commission on Cancer Research. We thank Xin Rong for input and advice. We thank Sheng (Tony) Hui, Cholsoon Jang, Li Chen, Yihui Shen, Lin Wang, Caroline Bartman, and all other Rabinowitz lab members for advice.

References

1. Lehninger AL, Nelson DL, Cox MM. Lehninger principles of biochemistry 6th ed. W.H. Freeman; 2013.
2. Yu Y, Clippinger AJ, Alwine JC. Viral effects on metabolism: changes in glucose and glutamine utilization during human cytomegalovirus infection. Trends Microbiol 7 2011;19(7):360–7. doi:10.1016/j.tim.2011.04.002 [PubMed: 21570293]
3. Heaton NS, Perera R, Berger KL, et al. Dengue virus nonstructural protein 3 redistributes fatty acid synthase to sites of viral replication and increases cellular fatty acid synthesis. Proc Natl Acad Sci U S A 10 2010;107(40):17345–50. doi:10.1073/pnas.1010811107 [PubMed: 20855599]
4. Singh A, Ruiz C, Bhalla K, et al. De novo lipogenesis represents a therapeutic target in mutant Kras non-small cell lung cancer. FASEB J 6 2018:fj201800204. doi:10.1096/fj.201800204 [PubMed: 29906244]
5. Stoiber K, Nagło O, Pernpeintner C, et al. Targeting de novo lipogenesis as a novel approach in anti-cancer therapy. Br J Cancer 1 2018;118(1):43–51. doi:10.1038/bjc.2017.374 [PubMed: 29112683]
6. Lambert JE, Ramos-Roman MA, Browning JD, Parks EJ. Increased de novo lipogenesis is a distinct characteristic of individuals with nonalcoholic fatty liver disease. Gastroenterology 3 2014;146(3):726–35. doi:10.1053/j.gastro.2013.11.049 [PubMed: 24316260]
7. Bence KK, Birnbaum MJ. Metabolic drivers of non-alcoholic fatty liver disease. Mol Metab 12 2020:101143. doi:10.1016/j.molmet.2020.101143 [PubMed: 33346069]
8. Jang C, Wada S, Yang S, et al. The small intestine shields the liver from fructose-induced steatosis. Nat Metab 7 2020;2(7):586–593. doi:10.1038/s42255-020-0222-9 [PubMed: 32694791]
9. Goldberg RP, Brunengraber H. Contributions of cytosolic and mitochondrial acetyl-CoA syntheses to the activation of lipogenic acetate in rat liver. Adv Exp Med Biol 1980;132:413–8. doi:10.1007/978-1-4757-1419-7_41 [PubMed: 6106997]
10. Hellerstein MK, Wu K, Kaempfer S, Kletke C, Shackleton CH. Sampling the lipogenic hepatic acetyl-CoA pool in vivo in the rat. Comparison of xenobiotic probe to values predicted from isotopomeric distribution in circulating lipids and measurement of lipogenesis and acetyl-CoA dilution. J Biol Chem 6 1991;266(17):10912–9. [PubMed: 2040608]
11. Chen L, Zhang Z, Hoshino A, et al. NADPH production by the oxidative pentose-phosphate pathway supports folate metabolism. Nat Metab 3 2019;1:404–415. [PubMed: 31058257]
12. Ghergurovich JM, Esposito M, Chen Z, et al. Glucose-6-Phosphate Dehydrogenase Is Not Essential for K-Ras-Driven Tumor Growth or Metastasis. Cancer Res 9 2020;80(18):3820–3829. doi:10.1158/0008-5472.CAN-19-2486 [PubMed: 32661137]
13. Yoshida A Hemolytic anemia and G6PD deficiency. Science 2 1973;179(4073):532–7. doi:10.1126/science.179.4073.532 [PubMed: 4405605]
14. Fan J, Ye J, Kamphorst JJ, Shlomi T, Thompson CB, Rabinowitz JD. Quantitative flux analysis reveals folate-dependent NADPH production. Nature 6 2014;510(7504):298–302. doi:10.1038/nature13236 [PubMed: 24805240]
15. Liu L, Shah S, Fan J, Park JO, Wellen KE, Rabinowitz JD. Malic enzyme tracers reveal hypoxia-induced switch in adipocyte NADPH pathway usage. Nat Chem Biol 5 2016;12(5):345–52. doi:10.1038/nchembio.2047 [PubMed: 26999781]
16. Simopoulos AP. Essential fatty acids in health and chronic disease. Am J Clin Nutr 9 1999;70(3 Suppl):560S-569S. doi:10.1093/ajcn/70.3.560s [PubMed: 10479232]
17. KINGSBURY KJ, PAUL S, CROSSLEY A, MORGAN DM. The fatty acid composition of human depot fat. Biochem J 3 1961;78:541–50. doi:10.1042/bj0780541 [PubMed: 13756126]

18. Wadke M, Brunengraber H, Lowenstein JM, Dolhun JJ, Arsenault GP. Fatty acid synthesis by liver perfused with deuterated and tritiated water. Biochemistry 7 1973;12(14):2619–24. [PubMed: 4711470]
19. JUNGAS R FATTY ACID SYNTHESIS IN ADIPOSE TISSUE INCUBATED IN TRITIATED WATER. Article. Biochemistry 1968 1968;7(10):3708-&. doi:10.1021/bi00850a050 [PubMed: 5681472]
20. SEYAMA Y, KAWAGUCHI A, KASAMA T, et al. IDENTIFICATION OF SOURCES OF HYDROGEN-ATOMS IN FATTY-ACIDS SYNTHESIZED USING DEUTERATED WATER AND STEREOSPECIFICALLY DEUTERIUM LABELED NADPH BY GAS-CHROMATOGRAPHIC MASS-SPECTROMETRIC ANALYSIS. Article. Biomedical Mass Spectrometry 1978 1978;5(5):357–361. doi:10.1002/bms.1200050507 [PubMed: 26434]
21. Diraison F, Pachiaudi C, Beylot M. In vivo measurement of plasma cholesterol and fatty acid synthesis with deuterated water: determination of the average number of deuterium atoms incorporated. Metabolism 7 1996;45(7):817–21. [PubMed: 8692014]
22. Hellerstein MK, Christiansen M, Kaempfer S, et al. Measurement of de novo hepatic lipogenesis in humans using stable isotopes. J Clin Invest 5 1991;87(5):1841–52. doi:10.1172/JCI115206 [PubMed: 2022750]
23. McCabe BJ, Previs SF. Using isotope tracers to study metabolism: application in mouse models. Metab Eng 1 2004;6(1):25–35. doi:10.1016/j.ymben.2003.09.003 [PubMed: 14734253]
24. Zhang Z, Chen L, Liu L, Su X, Rabinowitz JD. Chemical Basis for Deuterium Labeling of Fat and NADPH. J Am Chem Soc 10 2017;139(41):14368–14371. doi:10.1021/jacs.7b08012 [PubMed: 28911221]
25. Hellerstein MK. No common energy currency: de novo lipogenesis as the road less traveled. Am J Clin Nutr 12 2001;74(6):707–8. doi:10.1093/ajcn/74.6.707 [PubMed: 11722948]
26. Hui S, Ghergurovich JM, Morscher RJ, et al. Glucose feeds the TCA cycle via circulating lactate. Nature 11 2017;551(7678):115–118. doi:10.1038/nature24057 [PubMed: 29045397]
27. Sanchez-Gurmaches J, Tang Y, Jespersen NZ, et al. Brown Fat AKT2 Is a Cold-Induced Kinase that Stimulates ChREBP-Mediated De Novo Lipogenesis to Optimize Fuel Storage and Thermogenesis. Cell Metab 1 2018;27(1):195–209.e6. doi:10.1016/j.cmet.2017.10.008 [PubMed: 29153407]
28. Vijayakumar A, Aryal P, Wen J, et al. Absence of Carbohydrate Response Element Binding Protein in Adipocytes Causes Systemic Insulin Resistance and Impairs Glucose Transport. Cell Rep 10 2017;21(4):1021–1035. doi:10.1016/j.celrep.2017.09.091 [PubMed: 29069585]
29. Hui S, Cowan AJ, Zeng X, et al. Quantitative Fluxomics of Circulating Metabolites. Cell Metab 10 2020;32(4):676–688.e4. doi:10.1016/j.cmet.2020.07.013 [PubMed: 32791100]
30. Faubert B, Li KY, Cai L, et al. Lactate Metabolism in Human Lung Tumors. Cell 10 2017;171(2):358–371.e9. doi:10.1016/j.cell.2017.09.019 [PubMed: 28985563]
31. Gladden LB. Lactate metabolism: a new paradigm for the third millennium. J Physiol 7 2004;558(Pt 1):5–30. doi:10.1113/jphysiol.2003.058701 [PubMed: 15131240]
32. Gladden LB. A lactatic perspective on metabolism. Med Sci Sports Exerc 3 2008;40(3):477–85. doi:10.1249/MSS.0b013e31815fa580 [PubMed: 18379210]
33. Mashimo T, Pichumani K, Vemireddy V, et al. Acetate is a bioenergetic substrate for human glioblastoma and brain metastases. Cell 12 2014;159(7):1603–14. doi:10.1016/j.cell.2014.11.025 [PubMed: 25525878]
34. Schug ZT, Peck B, Jones DT, et al. Acetyl-CoA synthetase 2 promotes acetate utilization and maintains cancer cell growth under metabolic stress. Cancer Cell 1 2015;27(1):57–71. doi:10.1016/j.ccell.2014.12.002 [PubMed: 25584894]
35. Comerford SA, Huang Z, Du X, et al. Acetate dependence of tumors. Cell 12 2014;159(7):1591–602. doi:10.1016/j.cell.2014.11.020 [PubMed: 25525877]
36. Huang Z, Zhang M, Plec AA, et al. ACSS2 promotes systemic fat storage and utilization through selective regulation of genes involved in lipid metabolism. Proc Natl Acad Sci U S A 10 2018;115(40):E9499–E9506. doi:10.1073/pnas.1806635115 [PubMed: 30228117]
37. Zhao S, Jang C, Liu J, et al. Dietary fructose feeds hepatic lipogenesis via microbiota-derived acetate. Nature 3 2020;579(7800):586–591. doi:10.1038/s41586-020-2101-7 [PubMed: 32214246]

38. Nelson ME, Lahiri S, Chow JD, et al. Inhibition of hepatic lipogenesis enhances liver tumorigenesis by increasing antioxidant defence and promoting cell survival. Nat Commun 3 2017;8:14689. doi:10.1038/ncomms14689 [PubMed: 28290443]
39. Tasdogan A, Faubert B, Ramesh V, et al. Metabolic heterogeneity confers differences in melanoma metastatic potential. Nature 01 2020;577(7788):115–120. doi:10.1038/s41586-019-1847-2 [PubMed: 31853067]
40. Uhlén M, Fagerberg L, Hallström BM, et al. Proteomics. Tissue-based map of the human proteome. Science 1 2015;347(6220):1260419. doi:10.1126/science.1260419 [PubMed: 25613900]
41. Lewis CA, Parker SJ, Fiske BP, et al. Tracing compartmentalized NADPH metabolism in the cytosol and mitochondria of mammalian cells. Mol Cell 7 2014;55(2):253–63. doi:10.1016/j.molcel.2014.05.008 [PubMed: 24882210]
42. Ölander M, Wiśniewski JR, Artursson P. Cell-type-resolved proteomic analysis of the human liver. Liver Int 07 2020;40(7):1770–1780. doi:10.1111/liv.14452 [PubMed: 32243721]
43. Ding C, Li Y, Guo F, et al. A Cell-type-resolved Liver Proteome. Mol Cell Proteomics 10 2016;15(10):3190–3202. doi:10.1074/mcp.M116.060145 [PubMed: 27562671]
44. Battistuzzi G, D'Urso M, Toniolo D, Persico GM, Luzzatto L. Tissue-specific levels of human glucose-6-phosphate dehydrogenase correlate with methylation of specific sites at the 3' end of the gene. Proc Natl Acad Sci U S A 3 1985;82(5):1465–9. doi:10.1073/pnas.82.5.1465 [PubMed: 3856275]
45. Hao Q, Yadav R, Basse AL, et al. Transcriptome profiling of brown adipose tissue during cold exposure reveals extensive regulation of glucose metabolism. Am J Physiol Endocrinol Metab 3 01 2015;308(5):E380–92. doi:10.1152/ajpendo.00277.2014 [PubMed: 25516548]
46. Karlsson M, Zhang C, Méar L, et al. A single-cell type transcriptomics map of human tissues. Sci Adv 7 2021;7(31)doi:10.1126/sciadv.abh2169
47. Metallo CM, Gameiro PA, Bell EL, et al. Reductive glutamine metabolism by IDH1 mediates lipogenesis under hypoxia. Nature 11 2011;481(7381):380–4. doi:10.1038/nature10602 [PubMed: 22101433]
48. MacParland SA, Liu JC, Ma XZ, et al. Single cell RNA sequencing of human liver reveals distinct intrahepatic macrophage populations. Nat Commun 10 22 2018;9(1):4383. doi:10.1038/s41467-018-06318-7 [PubMed: 30348985]
49. Davidson SM, Papagiannakopoulos T, Olenchock BA, et al. Environment Impacts the Metabolic Dependencies of Ras-Driven Non-Small Cell Lung Cancer. Cell Metab 3 2016;23(3):517–28. doi:10.1016/j.cmet.2016.01.007 [PubMed: 26853747]
50. Piskounova E, Agathocleous M, Murphy MM, et al. Oxidative stress inhibits distant metastasis by human melanoma cells. Nature 11 2015;527(7577):186–91. doi:10.1038/nature15726 [PubMed: 26466563]
51. MacFarlane AJ, Liu X, Perry CA, et al. Cytoplasmic serine hydroxymethyltransferase regulates the metabolic partitioning of methylenetetrahydrofolate but is not essential in mice. J Biol Chem 9 2008;283(38):25846–53. doi:10.1074/jbc.M802671200 [PubMed: 18644786]
52. Ducker GS, Chen L, Morscher RJ, et al. Reversal of Cytosolic One-Carbon Flux Compensates for Loss of the Mitochondrial Folate Pathway. Cell Metab 10 2016;24(4):640–641. doi:10.1016/j.cmet.2016.09.011 [PubMed: 27732838]
53. Ducker GS, Ghergurovich JM, Mainolfi N, et al. Human SHMT inhibitors reveal defective glycine import as a targetable metabolic vulnerability of diffuse large B-cell lymphoma. Proc Natl Acad Sci U S A 10 2017;114(43):11404–11409. doi:10.1073/pnas.1706617114 [PubMed: 29073064]
54. Beaudin AE, Abarinov EV, Noden DM, et al. Shmt1 and de novo thymidylate biosynthesis underlie folate-responsive neural tube defects in mice. Am J Clin Nutr 4 2011;93(4):789–98. doi:10.3945/ajcn.110.002766 [PubMed: 21346092]
55. Meiser J, Tumanov S, Maddocks O, et al. Serine one-carbon catabolism with formate overflow. Sci Adv 10 2016;2(10):e1601273. doi:10.1126/sciadv.1601273 [PubMed: 27819051]
56. Zheng Y, Lin TY, Lee G, et al. Mitochondrial One-Carbon Pathway Supports Cytosolic Folate Integrity in Cancer Cells. Cell 11 2018;175(6):1546–1560.e17. doi:10.1016/j.cell.2018.09.041 [PubMed: 30500537]

57. Appling DR. Compartmentation of folate-mediated one-carbon metabolism in eukaryotes. FASEB J 9 1991;5(12):2645–51. doi:10.1096/fasebj.5.12.1916088 [PubMed: 1916088]
58. Barlowe CK, Appling DR. In vitro evidence for the involvement of mitochondrial folate metabolism in the supply of cytoplasmic one-carbon units. Biofactors 7 1988;1(2):171–6. [PubMed: 2475123]
59. Softic S, Meyer JG, Wang GX, et al. Dietary Sugars Alter Hepatic Fatty Acid Oxidation via Transcriptional and Post-translational Modifications of Mitochondrial Proteins. Cell Metab 10 2019;30(4):735–753.e4. doi:10.1016/j.cmet.2019.09.003 [PubMed: 31577934]
60. Alwahsh SM, Gebhardt R. Dietary fructose as a risk factor for non-alcoholic fatty liver disease (NAFLD). Arch Toxicol 4 2017;91(4):1545–1563. doi:10.1007/s00204-016-1892-7 [PubMed: 27995280]
61. Hellerstein MK, Schwarz JM, Neese RA. Regulation of hepatic de novo lipogenesis in humans. Annu Rev Nutr 1996;16:523–57. doi:10.1146/annurev.nu.16.070196.002515 [PubMed: 8839937]
62. Cohen P, Miyazaki M, Socci ND, et al. Role for stearoyl-CoA desaturase-1 in leptin-mediated weight loss. Science 7 2002;297(5579):240–3. doi:10.1126/science.1071527 [PubMed: 12114623]
63. Ducker GS, Rabinowitz JD. One-Carbon Metabolism in Health and Disease. Cell Metab 1 2017;25(1):27–42. doi:10.1016/j.cmet.2016.08.009 [PubMed: 27641100]
64. Mullarky E, Xu J, Robin AD, et al. Inhibition of 3-phosphoglycerate dehydrogenase (PHGDH) by indole amides abrogates de novo serine synthesis in cancer cells. Bioorg Med Chem Lett 9 2019;29(17):2503–2510. doi:10.1016/j.bmcl.2019.07.011 [PubMed: 31327531]
65. Pacold ME, Brimacombe KR, Chan SH, et al. A PHGDH inhibitor reveals coordination of serine synthesis and one-carbon unit fate. Nat Chem Biol 6 2016;12(6):452–8. doi:10.1038/nchembio.2070 [PubMed: 27110680]
66. Locasale JW. Serine, glycine and one-carbon units: cancer metabolism in full circle. Nat Rev Cancer 8 2013;13(8):572–83. doi:10.1038/nrc3557 [PubMed: 23822983]
67. Yang M, Vousden KH. Serine and one-carbon metabolism in cancer. Nat Rev Cancer 10 2016;16(10):650–62. doi:10.1038/nrc.2016.81 [PubMed: 27634448]
68. Ye J, Fan J, Venneti S, et al. Serine catabolism regulates mitochondrial redox control during hypoxia. Cancer Discov 12 2014;4(12):1406–17. doi:10.1158/2159-8290.CD-14-0250 [PubMed: 25186948]
69. Fu X, Deja S, Fletcher JA, et al. Measurement of lipogenic flux by deuterium resolved mass spectrometry. Nat Commun 6 18 2021;12(1):3756. doi:10.1038/s41467-021-23958-4 [PubMed: 34145255]
70. Wallace M, Metallo CM. Tracing insights into de novo lipogenesis in liver and adipose tissues. Semin Cell Dev Biol 12 2020;108:65–71. doi:10.1016/j.semcdb.2020.02.012 [PubMed: 32201132]
71. Strawford A, Antelo F, Christiansen M, Hellerstein MK. Adipose tissue triglyceride turnover, de novo lipogenesis, and cell proliferation in humans measured with 2H2O. Am J Physiol Endocrinol Metab 4 2004;286(4):E577–88. doi:10.1152/ajpendo.00093.2003 [PubMed: 14600072]
72. Shi Y, Pizzini J, Wang H, et al. -Adrenergic receptor agonist induced hepatic steatosis in mice: modeling nonalcoholic fatty liver disease in hyperadrenergic states. Am J Physiol Endocrinol Metab 7 01 2021;321(1):E90–E104. doi:10.1152/ajpendo.00651.2020 [PubMed: 34029162]
73. Brunengraber H, Kelleher JK, Des Rosiers C. Applications of mass isotopomer analysis to nutrition research. Annu Rev Nutr 1997;17:559–96. doi:10.1146/annurev.nutr.17.1.559 [PubMed: 9240940]
74. Laugero KD, Moberg GP. Energetic response to repeated restraint stress in rapidly growing mice. Am J Physiol Endocrinol Metab 7 2000;279(1):E33–43. doi:10.1152/ajpendo.2000.279.1.E33 [PubMed: 10893320]
75. Svensson RU, Parker SJ, Eichner LJ, et al. Inhibition of acetyl-CoA carboxylase suppresses fatty acid synthesis and tumor growth of non-small-cell lung cancer in preclinical models. Nat Med 10 2016;22(10):1108–1119. doi:10.1038/nm.4181 [PubMed: 27643638]
76. Esler WP, Bence KK. Metabolic Targets in Nonalcoholic Fatty Liver Disease. Cell Mol Gastroenterol Hepatol 2019;8(2):247–267. doi:10.1016/j.jcmgh.2019.04.007 [PubMed: 31004828]

77. Kim CW, Addy C, Kusunoki J, et al. Acetyl CoA Carboxylase Inhibition Reduces Hepatic Steatosis but Elevates Plasma Triglycerides in Mice and Humans: A Bedside to Bench Investigation. Cell Metab 9 2017;26(3):576. doi:10.1016/j.cmet.2017.08.011 [PubMed: 28877461]

78. Goedeke L, Bates J, Vatner DF, et al. Acetyl-CoA Carboxylase Inhibition Reverses NAFLD and Hepatic Insulin Resistance but Promotes Hypertriglyceridemia in Rodents. Hepatology 12 2018;68(6):2197–2211. doi:10.1002/hep.30097 [PubMed: 29790582]

79. Chondronikola M, Volpi E, Børsheim E, et al. Brown adipose tissue improves whole-body glucose homeostasis and insulin sensitivity in humans. Diabetes 12 2014;63(12):4089–99. doi:10.2337/db14-0746 [PubMed: 25056438]

80. Stanford KI, Middelbeek RJ, Townsend KL, et al. Brown adipose tissue regulates glucose homeostasis and insulin sensitivity. J Clin Invest 1 2013;123(1):215–23. doi:10.1172/JCI62308 [PubMed: 23221344]

81. Tuli JS, Smith JA, Morton DB. Stress measurements in mice after transportation. Lab Anim 4 1995;29(2):132–8. doi:10.1258/002367795780740249 [PubMed: 7602999]

82. Rong X, Albert CJ, Hong C, et al. LXRs regulate ER stress and inflammation through dynamic modulation of membrane phospholipid composition. Cell Metab 11 2013;18(5):685–97. doi:10.1016/j.cmet.2013.10.002 [PubMed: 24206663]

83. Jang C, Hui S, Zeng X, et al. Metabolite Exchange between Mammalian Organs Quantified in Pigs. Cell Metab 6 2019;doi:10.1016/j.cmet.2019.06.002

84. Chen L, Ducker GS, Lu W, Teng X, Rabinowitz JD. An LC-MS chemical derivatization method for the measurement of five different one-carbon states of cellular tetrahydrofolate. Anal Bioanal Chem 10 2017;409(25):5955–5964. doi:10.1007/s00216-017-0514-4 [PubMed: 28799108]

85. Melamud E, Vastag L, Rabinowitz JD. Metabolomic analysis and visualization engine for LC-MS data. Anal Chem 12 2010;82(23):9818–26. doi:10.1021/ac1021166 [PubMed: 21049934]

86. Su X, Lu W, Rabinowitz JD. Metabolite Spectral Accuracy on Orbitraps. Anal Chem 5 2017;doi:10.1021/acs.analchem.7b00396

87. Shah V, Herath K, Previs SF, Hubbard BK, Roddy TP. Headspace analyses of acetone: a rapid method for measuring the 2H-labeling of water. Anal Biochem 9 2010;404(2):235–7. doi:10.1016/j.ab.2010.05.010 [PubMed: 20488158]

88. Eipel C, Abshagen K, Vollmar B. Regulation of hepatic blood flow: the hepatic arterial buffer response revisited. World J Gastroenterol 12 2010;16(48):6046–57. doi:10.3748/wjg.v16.i48.6046 [PubMed: 21182219]

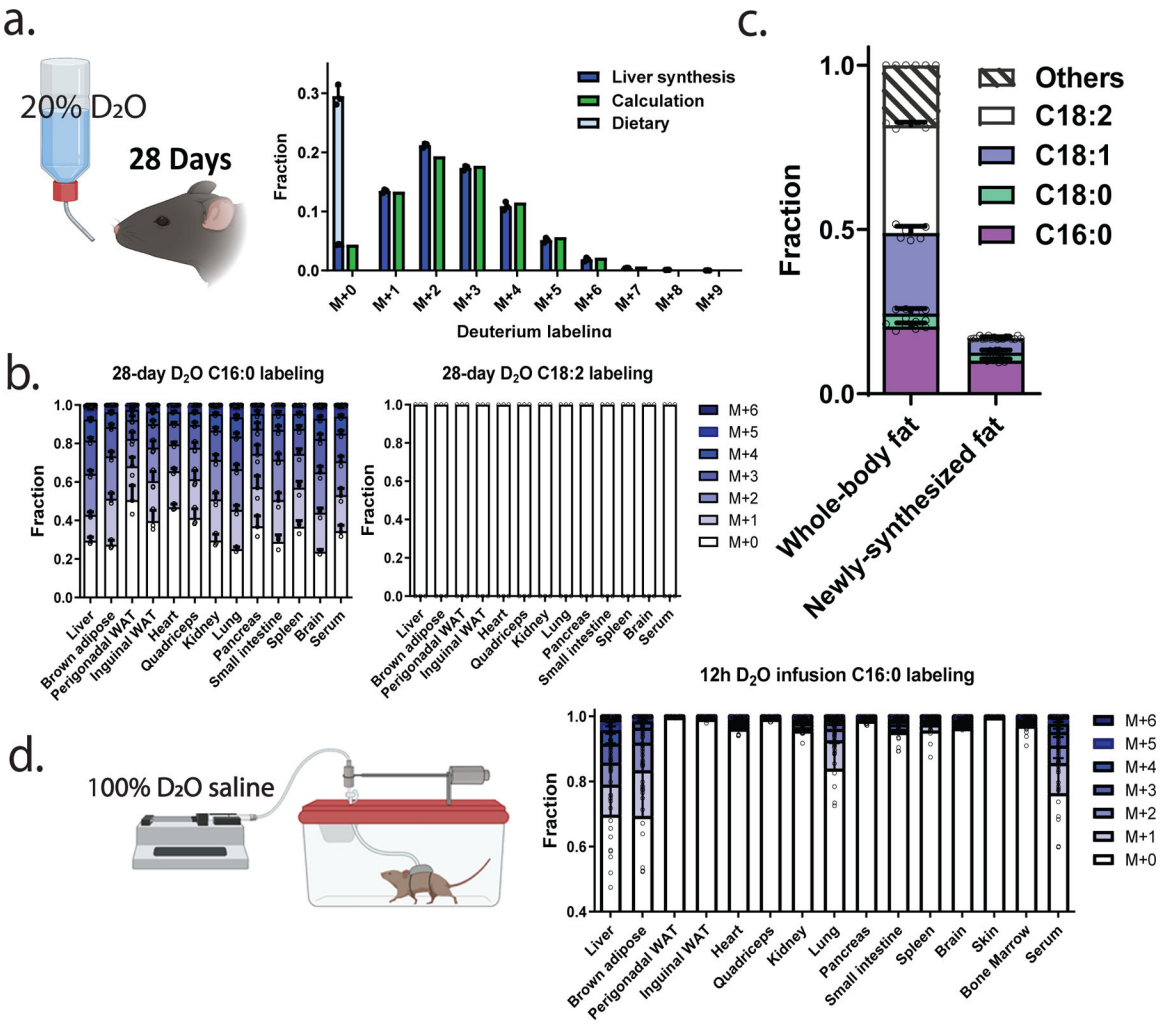

Figure 1. *De novo* lipogenesis in liver and brown adipose produces much of whole-body saturated fat

a. Liver palmitate (C16:0) labeling pattern after 4 weeks of D_2O drinking. Left bars (blue) reflect the experimentally observed labeling; right bars (green) reflect the calculated labeling based on fraction of newly synthesized fat and observed D_2O and NADPH labeling. Fraction dietary versus synthesized fat is based on fitting the labeling pattern. Throughout the manuscript, all data are for saponified fatty acids.

b. Palmitate (C16:0) and linoleate (C18:2) labeling pattern across tissues after 4 weeks D_2O drinking. C18:2 is an essential fatty acid and accordingly shows no labeling.

c. Composition of whole-body fat (left) and fraction that is endogenously synthesized based on the 4-week D_2O drinking data (right).

d. C16:0 labeling pattern across tissues after 12 h fed-state D_2O infusion.

Mean ± s.d., n=6 mice for composition analysis (3 males and 3 females); n=3 males for D_2O drinking experiment and n=10 (5 males and 5 females) for 12 h D_2O infusion. Images in a and d were created with BioRender.com.

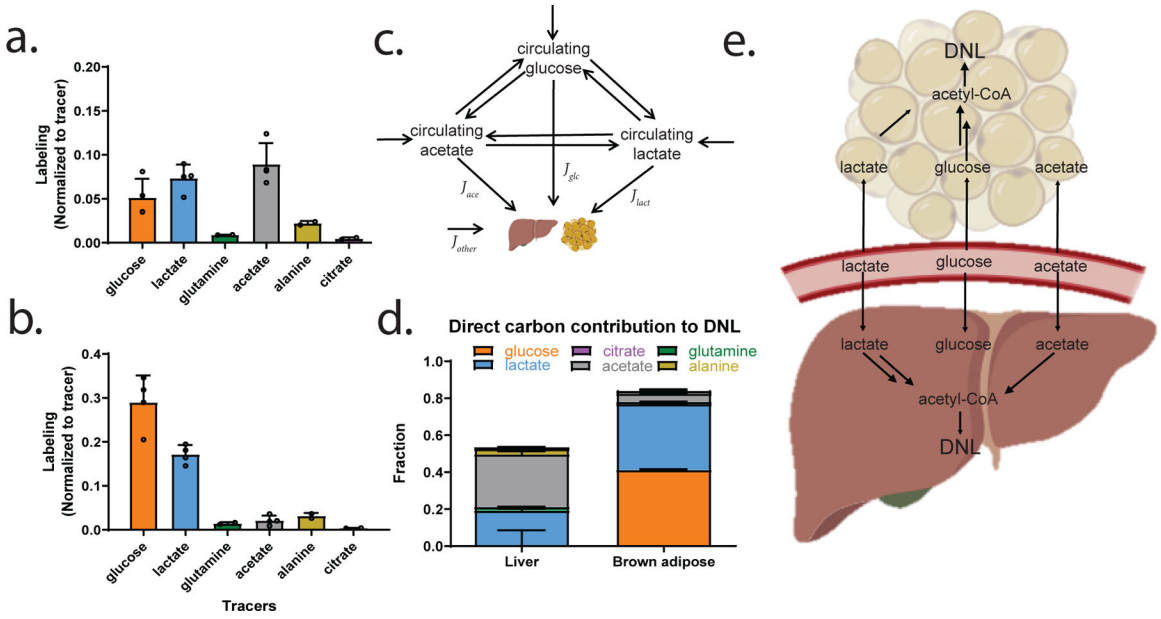

Figure 2. Liver and brown adipose use different carbon sources to support lipogenesis

a. Average atom labeling of liver C16:0 following 12 h infusion of [U-^{13}C]-labeled glucose (n=4), lactate (n=4), glutamine (n=2), acetate (n=4), alanine (n=2) and citrate (n=2). Labeling is normalized to circulating tracer labeling. Brown adipose is perfused by systemic blood (approximated by tail vein sampling) and liver by 78% portal vein blood and 22% systemic blood.

b. As is (a), for brown adipose C16:0.

c. Isotope tracing into fat is complicated by interconversion of the tracer with other circulating metabolites. By conducting tracer experiments with all key circulating substrates, the direct contribution of each can be determined by linear algebra.

d. Carbon sources supporting *de novo* lipogenesis in liver and brown adipose, based on direct contributions to C16:0, calculated based on data in (a) and (b) and Sup. 2.

e. Schematic of differential lipogenic substrate use by liver versus brown adipose.

Data in a, b are mean ± s.d.; data in d is mean ± s.e.m. All mice are males. Results in females are similar (Sup. 6). Images in c and e were created with BioRender.com

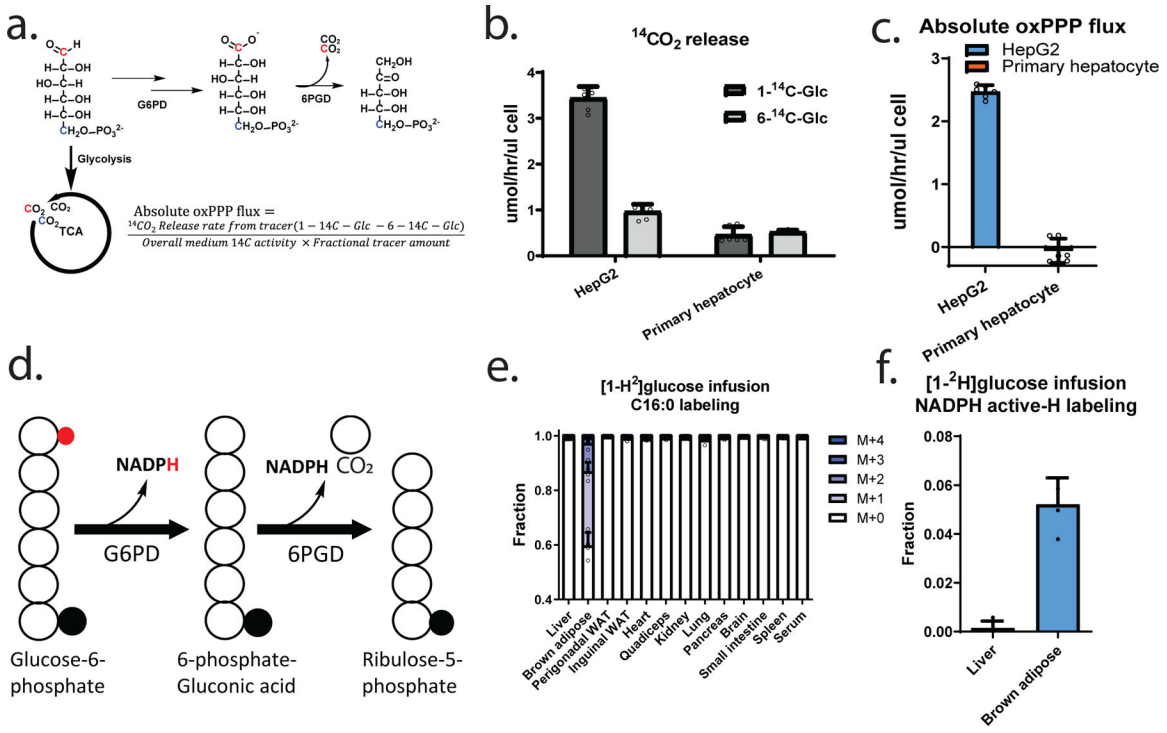

Figure 3. Brown adipose generates lipogenic NADPH via the oxPPP but not liver

a. Scheme for ^{14}C experiment to examine absolute oxPPP flux.

b. $^{14}CO_2$ release flux from [1-^{14}C]glucose and [6-^{14}C]glucose in HepG2 and primary hepatocytes.

c. Absolute oxPPP flux in HepG2 and primary hepatocytes.

d. Schematic of pathway by which [1-^{2}H]glucose labels NADPH via the oxPPP.

e. C16:0 labeling across tissues following 12 h [1-^{2}H]glucose infusion (125 nmol/min/gram body weight).

f. NADPH active-H measurement in liver and brown adipose from 12 h [1-^{2}H]glucose infusion (125 nmol/min/gram bw).

Mean ± s.d., n=6 replicates for cultured cell experiments; n=4 mice for [1-^{2}H]glucose infusion. All mice are males. Results in females are similar (Sup. 6).

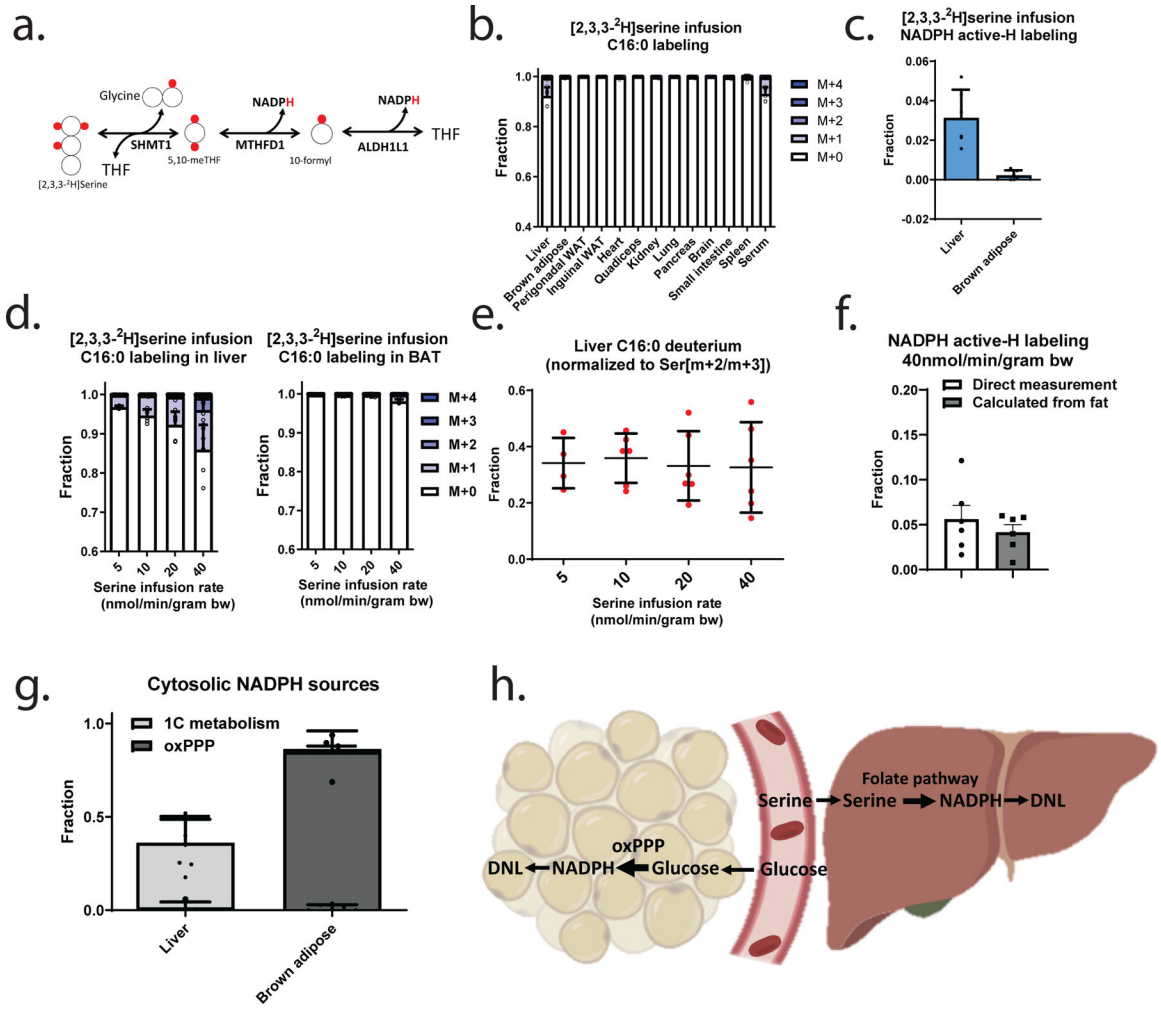

Figure 4. Serine's hydride contribution to liver fat across 8-fold range of [2,3,3-^{2}H]serine infusion rates

a. Schematic of pathway by which [2,3,3-^{2}H]serine labels NADPH via cytosolic folate metabolism.

b. C16:0 labeling across tissues following 12 h [2,3,3-^{2}H]serine infusion (20 nmol/min/gram bw)

c. NADPH active-H measurement in liver and brown adipose from 12 h [2,3,3-^{2}H]serine infusion (20 nmol/min/gram bw)

d. Liver and brown adipose tissue C16:0 labeling following 12h [2,3,3-^{2}H]serine infusion at different rates, ranging from minimally to highly perturbative.

e. Corresponding normalized contribution of serine to liver C16:0 hydrogen (average number of labeled hydrogens in C16:0 relative to fraction serine M+2 or M+3).

f. NADPH active-H labeling following 12h [2,3,3-^{2}H]serine infusion at 40nmol/min/gram bodyweight measured either directly (from Sup.5f) or calculated from palmitate (from Fig.4d left).

g. Hydride sources supporting *de novo* lipogenesis in liver and brown adipose, correcting for substrate labeling and H-D exchange between NADPH and water. Calculated based on tracer data in (c) and (f) and D_2O exchange data in Sup. 4f.

h. Schematic of differential lipogenic substrate use by liver versus brown adipose.
All data are mean ± s.d., n=4 for 5 nmol/min/gram bodyweight and n=6 for 10, 20 and 40 nmol/min/gram bodyweight of [2,3,3-^{2}H]serine infusion. All mice are males. Panel h was created with BioRender.com.

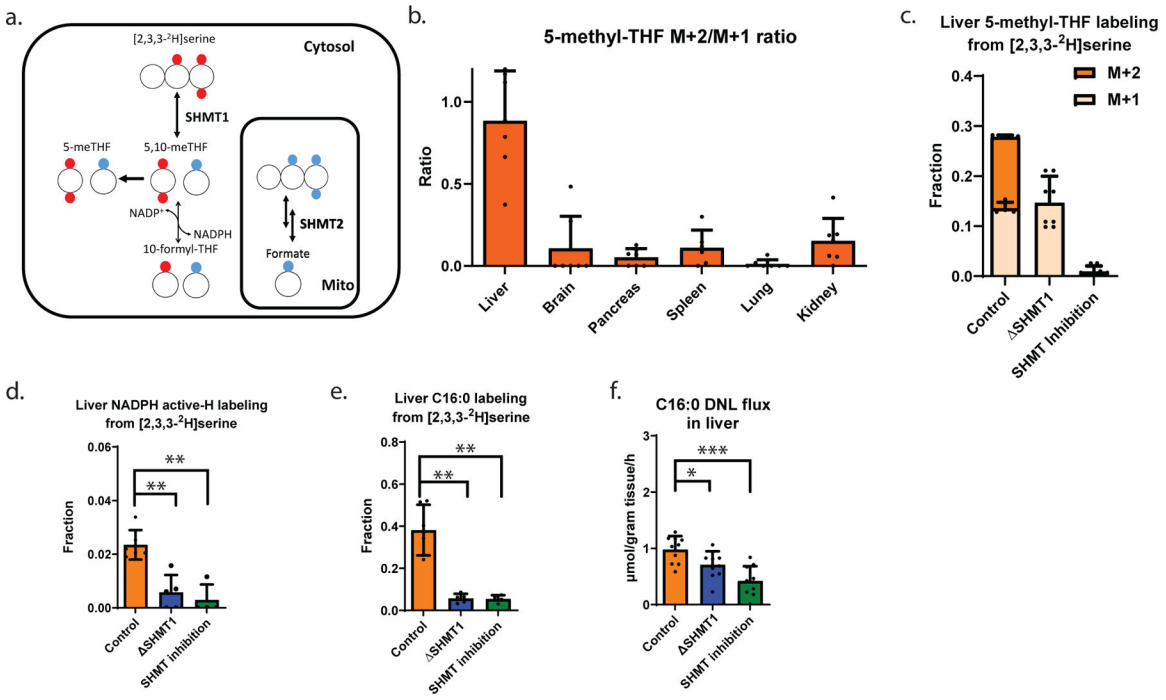

Figure 5. Liver serine catabolism generates NADPH via SHMT1-MTHFD1-ALDH1L1 and thereby supports hepatic lipogenesis

a. Schematic of the cytosolic and mitochondrial serine catabolic pathways. Metabolite labeling from [2,3,3-^{2}H]serine generated by the cytosolic pathway is shown in red and mitochondrial pathway in blue.

b. 5-methyl-THF labeling for 12 h [2,3,3-^{2}H]serine infusion (20 nmol/min/gram body weight). Ratio of M+2 to M+1 labeling reflects relative contribution of cytosolic versus mitochondrial serine catabolism to 1C units in 5-methyl-THF.

c. 5-methyl-THF labeling in liver for 12 h [2,3,3-^{2}H]serine infusion (20 nmol/min/gram bw) in control, whole-body ΔSHMT1 mice, and mice treated with the dual SHMT1/2 inhibitor SHIN2 (3.33 mg/kg/h i.v. infusion).

d. NADPH active-H measurement in liver for 12 h [2,3,3-^{2}H]serine infusion (20 nmol/min/gram bw) (control vs. ΔSHMT1, p=0.0048; control vs. SHIN2 treatment, p=0.0043).

e. C16:0 labeling in liver for 12 h [2,3,3-^{2}H]serine infusion (20 nmol/min/gram bw). Labeling is normalized to liver serine enrichment and reported as the average number of labeled hydrogens in C16:0. (control vs. ΔSHMT1, p=0.0043; control vs. SHIN2 treatment, p=0.0095).

f. C16:0 lipogenesis flux in liver overnight, as measured by 12 h D_2O infusion (control vs. ΔSHMT1, p=0.043; control vs. SHIN2 treatment, p=0.0002).

Mean ± s.d. For serine tracing, n=6 for control, n=5 for ΔSHMT1, n=4 for inhibitor treatment. For D_2O infusion in (f) and (g), n=10 for all 3 conditions, in (h) n=6 for vehicle control, n=7 for SHIN2 treatment. All mice are males. *p<0.05, **p<0.01; ***p<0.005 by unpaired Mann-Whitney test, all p-values are two-sided.

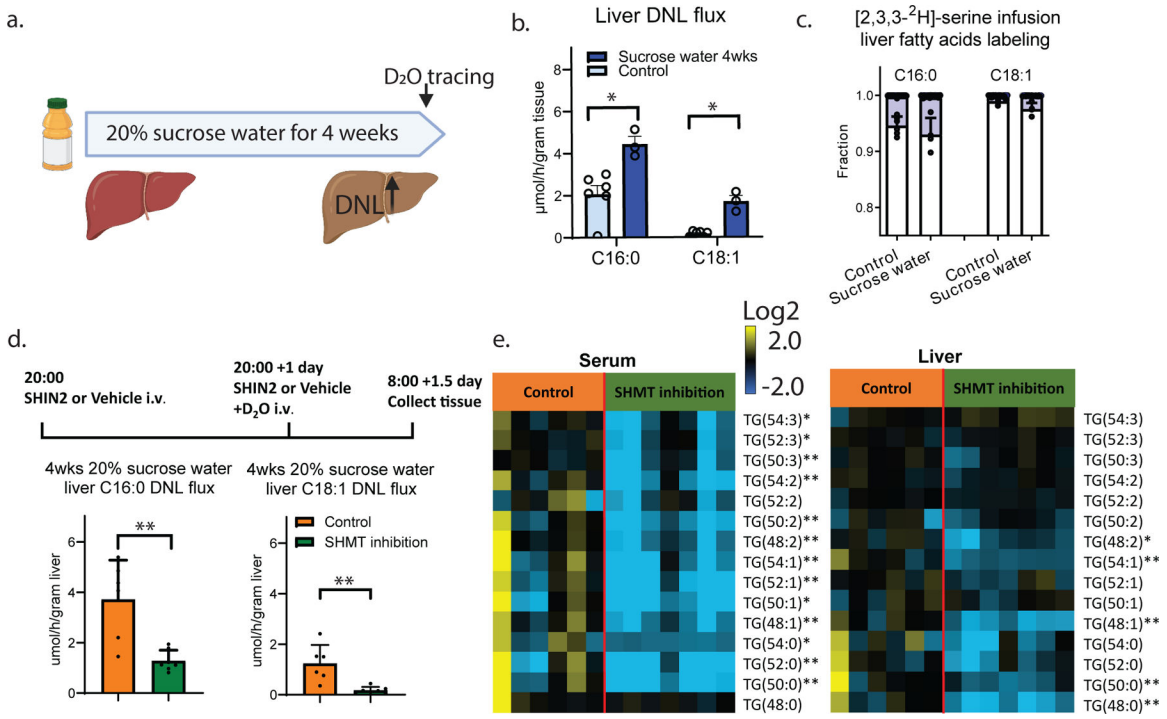

Figure 6. Sucrose-induced lipogenesis consumes hydride from serine and depends on SHMT activity

a. C16:0 and C18:1 lipogenesis flux in liver of control and 4 weeks 20% sucrose water drinking mice (control vs. sucrose water drinking, p=0.024 for liver C16:0, p=0.024 for liver C18:1).

b. C16:0 and C18:1 labeling from 12 h [2,3,3-^{2}H]serine infusion (10 nmol/min/gram body weight) in control and 4 weeks 20% sucrose water drinking mice.

c. Impact of pharmacological SHMT1/2 inhibition on sucrose-induced lipogenesis. Mice were given 20% sucrose in the drinking water for 4 weeks. Then, 36 h prior to sacrifice and tissue collection, they were given vehicle or SHIN2 (3.33 mg/kg/h i.v. infusion). The SHIN2 or vehicle infusion was then augmented by D_2O infusion for the final 12 h, which corresponded to the fed state (nighttime). Lipogenesis with or without SHIN2 treatment is shown. (Control vs. SHIN2 treatment, p=0.0047 for C16:0; p=0.0023 for C18:1).

d. Serum and hepatic TG levels with or without SHIN2 treatment, in heatmap format. (Control vs. SHIN2 treatment, for serum, TG(48:0) p=0.23, TG(50:0) p=0.0012, TG(52:0) p=0.0047, TG(54:0) p=0.0221, TG(48:1) p=0.0023, TG(50:1) p=0.014, TG(52:1) p=0.0047, TG(54:1) p=0.0082, TG(48:2) p=0.0012, TG(50:2) p=0.0023, TG(52:2) p=0.29, TG(54:2) p=0.0082, TG(50:3) p=0.0082, TG(52:3) p=0.035, TG(54:3) p=0.014. For liver, TG(48:0) p=0.0012, TG(50:0) p=0.0082, TG(52:0) p=0.051, TG(54:0) p=0.051, TG(48:1) p=0.0012, TG(50:1) p=0.94, TG(52:1) p=0.14, TG(54:1) p=0.0012, TG(48:2) p=0.014, TG(50:2) p=0.53, TG(52:2) p=0.073, TG(54:2) p=0.23, TG(50:3) p=0.14, TG(52:3) p=0.63, TG(54:3) p=0.051).

Mean± s.d. For experiments comparing control to sucrose water drinking, n=6 for control, n=3 for 4-week sucrose water drinking. For experiments comparing vehicle to SHIN2 treatment, n=6 for control and n=7 for SHIN2. *p<0.05; **p<0.01; ***p<0.005 by unpaired

Mann-Whitney test, all statistic-values are two-sided. All mice are males. Panel a was created with BioRender.com.

Table 1.

Tracer infusion parameters.

Tracer	Conc.	Infusion rate (ul/min/gram bodyweight)	Infusion flux (nmol/min/gram bodyweight)
D_2O	100%	0.2	
[2,3,3-^{2}H]serine	400mM 200mM 100mM 50mM	0.1	40 20 10 5
[1-^{2}H]glucose	625mM	0.2	125
[2,3,3,4,4-^{2}H]glutamine	150mM	0.2	30
[U-^{2}H]formate	80mM	0.1	8
[U^{13}C]glucose	400mM	0.2	80
[U^{13}C]sodium lactate	5% W/W	0.1	45
[U^{13}C]sodium acetate	150mM	0.1	15
[U^{13}C]glutamine	170mM	0.1	17
[U^{13}C]alanine	300mM	0.1	30
[U^{13}C]citrate	20mM	0.1	2